Determination of a conformational change in filamin A with Förster resonance energy transfer

Master's Thesis

University of Jyväskylä
Department of Biological and Environmental Science
Cell and Molecular Biology

18.5.2011

Jonne Seppälä

Preface

This study was conducted in the group of professor Jari Ylänne at the University of Jyväskylä, Department of Biological and Environmental Science, Division of Molecular Recognition during June 2010 and May 2011.

First of all, I would like to thank professor Jari Ylänne for the supervision and opportunity to work as a part of the group. I also thank adjunct professor Ulla Pentikäinen for excellent supervision and sharing of gray hairs during the experimental procedures. Furthermore, this thesis would not have completed without the help of professor Janne Ihalainen and his expertise on spectroscopy. A special thanks go also to laboratory technician Arja "Allu" Mansikkaviita for technical assistance, time-saving tips, and engouragement along the way. I express my deepest gratitudes to Emmi for baring with me during the long days writing this thesis. I am also very grateful for the support from my family during these years. Finally, I would like to thank the Academy of Finland for funding this project.

Jyväskylä, May 2011

Jonne Seppälä

University of Jyväskylä
Faculty of mathematics and Science

Abstract of Master's Thesis

Author: Jonne Seppälä
Title of thesis: Determination of a conformational change in filamin A with Förster resonance energy transfer
Finnish title: Filamiini A:n konformaatiomuutoksen määrittäminen Försterin resonanssienergian-siirtoa hyödyntäen
Date: 18.5.2011 **Pages:** 46+1

Department: Department of Biological and environmental science
Chair: Cell and Molecular biology
Supervisors: Ulla Pentikäinen, Ph.D., adjunctant professor and Jari Ylänne, Ph.D., professor

---

Abstract:

Filamins are large rod-like proteins that cross-link actin filaments into three-dimensional networks. They also bind to a plethora of proteins with distinct functions showing that they have a versatile role in cells. Functional filamins are dimers consisting of an N-terminal actin binding domain followed by 24 immunoglobulin-like domains. The most C-terminal domains mediate the dimerization. Two hinge regions are located between the domains 15 and 16 and 23 and 24, respectively, and produce structural flexibility that is essential for the protein function. The domains 18-19 and 20-21 are folded in a pairwise manner in which the first β strands of the even numbered domains are folded along with the odd numbered domains. Recent study implies that a focal adhesion protein migfilin binding replaces the β strand of the domain 20 inducing a conformational change in filamin A that makes its structure more flexible. Previously only stretching force induced conformational changes have been reported and they are thought to function as a mechanism to sense tension. The aim of this study was to demonstrate the migfilin induced conformational change using Förster resonance energy transfer (FRET). Enhanced green fluorescent protein (EGFP) was cloned to the C-terminus of a four domain fragment of filamin A which was first mutated to have a unique site for the acceptor fluorophore conjugation. Then, the recombinant fusion protein was expressed overnight and subsequently purified with affinity chromatography and gel filtration. Finally, the purified protein was labeled with Alexa Fluor 532 C_5 maleimide to produce a FRET pair. The change in the energy transfer efficiency upon migfilin addition was measured with steady-state and time-resolved fluorescence methods. No statistically significant change in the amount of energy transfer was observed. The reason is unclear, though it is possible that the EGFP disrupted the dynamics of filamin A or that the migfilin binding was abolished. However, it is also possible that the used method was not sensitive for the possible conformational change in the construct. Changes in the construct are required in further studies.

Keywords: EGFP, filamin A, FRET

Jyväskylän yliopisto **Pro Gradu –tutkielman tiivistelmä**
Matemaattis-luonnontieteellinen tiedekunta

Tekijä: Jonne Seppälä
Tutkielman nimi: Filamiini A:n konformaatiomuutoksen määrittäminen Försterin resonanssienergian-siirtoa hyödyntäen
Englinsh title: Determination of a conformational change in filamin A with Förster resonance energy transfer
Päivämäärä: 18.5.2011 **Sivumäärä:** 46+1

Laitos: Bio- ja ympäristötieteiden laitos
Oppiaine: Solu- ja molekyylibiologia
Tutkielman ohjaajat: Ulla Pentikäinen, FT, dosentti ja Jari Ylänne, FT, professori

---

Tiivistelmä:

Filamiinit ovat suuria sauvamaisia proteiineja, jotka liittävät aktiinifilamentteja kolmiulotteisiksi verkostoiksi. Filamiineilla on monitahoinen rooli solussa, sillä ne sitovat lisäksi suurta joukkoa toiminnallisesti erilaisia proteiineja. Ihmisellä on kolme filamiinigeeniä: A, B ja C. Filamiinit ovat dimeerejä, joiden aminopäässä on aktiinia sitova domeeni, jota seuraa 24 immunoglobuliinin kaltaista domeenia. Filamiini dimerisoituu karboksiterminaalisesta päästä. Domeenien 15 ja 16 sekä 23 ja 24 välissä ovat sarana-alueet, jotka mahdollistavat proteiinin toiminnan kannalta tärkeän taipuisuuden. Domeenit 18-19 ja 20-21 laskostuvat pareittain siten, että parillisten domeenien ensimmäinen β-säie on laskostunut parittomien domeenien kanssa. Viimeaikainen tutkimus osoittaa että fokaaliadheesioproteiini migfiliinin sitoutuminen irrottaa domeenin 20 β-säikeen rakenteesta ja johtaa konformaatiomuutokseen, joka tekee filamiinista joustavamman. Aiemmin on raportoitu, että venyttävän voiman kohdistuminen filamiiniin johtaa konformaatiomuutoksiin, joiden on uskotaan toimivan säätelymekanismina, joka tunnistaa soluun kohdistuvaa jännitystä. Tutkimuksen tarkoituksena oli osoittaa migfiliinin sitoutumisen aiheuttama konformaatiomuutos hyödyntäen Försterin resonanssienergian siirtoa (*engl. Förster resonance energy transfer*, FRET). Filamiini A:n domeenit 18-21 mutatoitiin siten, että saatiin aikaiseksi spesifinen paikka akseptorifluoroforin konjugaatiolle. Tämän jälkeen vihreää fluoresoiva proteiini (*engl. Enhanced green fluorescent protein,* EGFP) kloonattiin filamiini A:n karboksipäähän. Proteiinia tuotettiin yön yli kasvatuksessa ja puhdistettiin affiniteettikromatografialla ja geelisuodatuksella. Lopulta puhdas proteiini leimattiin Alexa Fluor 532 C_5 maleidi -fluoroforilla, jotta saatiin aikaiseksi FRET-pari. Muutosta energiansiirron tehokkuudessa migfiliinin lisäyksen jälkeen seurattiin fluoresenssispektroskopialla sekä aikaerotteisella fluoresenssimittauksella. Tilastollisesti merkitsevää eroa energiansiirron tehokkuudessa ei havaittu. Syy on epäselvä, mutta on mahdollista että filamiini A:n dynamiikka kärsi EGFP:n vaikutuksesta tai että migfiliinin sitoutuminen oli estynyt. On lisäksi mahdollista ettei käytetty menetelmä ollut tarpeeksi herkkä havaitsemaan tässä konstruktissa mahdollisesti tapahtuvaa konformaatiomuutosta. Lisätutkimuksia varten proteiinikonstruktiin on tehtävä muutoksia.

Avainsanat: EGFP, filamiini A, FRET

Contents

Abbreviations **6**

1 Introduction **7**
1.1 Actin cytoskeleton . . . 7
1.2 Filamins . . . 7
1.2.1 Filamin family . . . 7
1.2.2 Overall structure of filamins . . . 8
Structure of actin binding domain . . . 8
Structure of immunoglobulin-like domains . . . 9
Structure of the dimerization domain . . . 11
1.3 Biological functions of filamins . . . 14
1.3.1 Filamins in cell motility and adhesion . . . 15
1.3.2 Filamins in signal transduction and transcriptional regulation . . . 16
1.4 Regulation of filamin associated interactions . . . 17
1.5 Filamin associated diseases . . . 18
1.5.1 Filamin A defects . . . 19
1.5.2 Filamin B and C defects . . . 19
1.6 Förster resonance energy transfer . . . 20

2 Aim of the study **23**

3 Materials and methods **24**
3.1 Mutagenesis and cloning . . . 24
3.2 Protein expression and purification . . . 25
3.3 Fluorophore labeling . . . 25
3.4 Steady-state and time-resolved fluorescence measurements . . . 26
3.5 Molecular dynamics simulations . . . 27

4 Results **29**
4.1 Protein purification and fluorophore labeling . . . 29
4.2 The effect of peptide addition to donor fluorescence emission . . . 29
4.3 The effect of peptide addition to donor fluorescence lifetime . . . 32
4.4 Molecular dynamics simulation structure of FLNa18-21-EGFP . . . 32

5 Discussion **35**
5.1 Peptide addition did not change the amount of energy transfer . . . 36
5.2 Distance calculations give insight to the orientation of the domain pairs . . . 38
5.3 Future perspectives . . . 39

References **41**

Abbreviations

ABD	actin binding domain
CH	calponin homology
EGFP	enhanced green fluorescent protein
filgap	filamin A-binding RhoGTPase activating protein
FLN	filamin
FRET	Förster resonance energy transfer
GPIbα	glycoprotein Ibα
MD	molecular dynamics
PDB	Protein Data Bank, http://www.rcsb.org/pdb
RMSD	root mean square deviation
SAXS	small angle X-ray scattering

1 Introduction

1.1 Actin cytoskeleton

Cytoskeleton is a complex protein organization that maintains cell shape and gives structural strength. It is not a stable structure, but is highly dynamic. Components of the cytoskeleton are hollow cylindrical microtubules, intermediate filaments – a mixed group of rodlike proteins with various subclasses, and microfilaments or actin filaments. Actin filaments assemble in branched three-dimensional networks that form actin cytoskeleton which plays a crucial role in maintaining cell shape as well as in migration, adhesion and organelle transport. Dynamics of actin cytoskeleton is regulated by plethora of actin binding proteins that modulate actin filament assembly and disassembly, branching and bundling.

1.2 Filamins

Filamins (FLNs) are large actin-binding proteins that crosslink actin filaments into three-dimensional networks and link them to membranes. Beside their role in the regulation of actin cytoskeleton, recent studies have revealed their involvement in cell signaling, regulation of transcription and organ development (for review see Zhou et al., 2010), thus pointing out that FLNs have versatile role in cells. FLN was originally isolated from chicken gizzard and named after its filamentous structure and colocalization with stress fibers (Wang et al., 1975).

1.2.1 Filamin family

The mammalian family of filamin genes encodes three proteins: FLNa, FLNb and FLNc (for review see van der Flier and Sonnenberg, 2001). FLNA is located in X chromosome, FLNB in chromosome three and FLNC in chromosome seven. All of the proteins have high identity, near 70%. The divergence is greater in the hinge regions that produce structural flexibility important for the function (figure 1). In addition, FLNc has an insertion not found from FLNa or b. The diversity of FLNs is further increased by alternative splicing, mainly affecting the ability of the rod two domains to bind their interacting partners (for review see van der Flier and Sonnenberg, 2001). FLNa and FLNb are widely expressed but FLNc is restricted to skeletal and cardiac

muscle cells (Thomson et al., 2000). FLN orthologues have also been found from *Drosophila melanogaster*, *Caenorhabditis elegans*, *Dictyostelium discoideum* and *Entamoeba histolytica* (for review see van der Flier and Sonnenberg, 2001).

The high identity of the proteins has led to the assumption of the existence of heterodimers (for review see Zhou et al., 2010). In mouse migratory neurons FLNa and FLNb form heterodimers during cortical development (Sheen et al., 2002), but several contradictory *in vitro* results have been reported and whether FLNs form stable heterodimers more widely need to be resolved. Heterodimerization could serve as a compensatory mechanism for other isoforms or even extend their functionality through isoform specific interacting partners (for review see Zhou et al., 2010).

1.2.2 Overall structure of filamins

Mammalian FLNs (figure 1) are V-shaped elongated proteins consisting of two approximately 280 kDa monomers (Gorlin et al., 1990). Each monomer consists of an N-terminal actin binding domain (ABD) followed by 24 Ig-like domains (Fucini et al., 1997). These domains are divided into two rods by two flexible hinge segments situated between Ig-like domains 15 and 16 and 23 and 24, respectively. The dimerization occurs via the most C-terminal Ig-like domains (Fucini et al., 1997).

Structure of actin binding domain The FLNa ABD (figure 2A) is composed of two calponin homology domains (CHs), CH1 and CH2, with three actin-binding sequences (Clark et al., 2009). Two of the sequences are located in CH1 and one in CH2. The sequences do not form a continuous surface indicating that structural rearrangements occur to allow complete binding of actin filaments or not all sequences bind actin filaments simultaneously (Clark et al., 2009).

The CH domain was originally found from actin binding protein calponin that regulates muscle contraction (for review see Korenbaum and Rivero, 2002). The CH domain is composed of four core α helices and one to three shorter α helices in the loops between the core. A pair of CH domains is needed to form a full ADB such as in filamins. Other actin filaments binding proteins containing similar ABDs are alpha-actinins, spectrins, dystrophin, and plakins (for review see Korenbaum and Rivero, 2002).

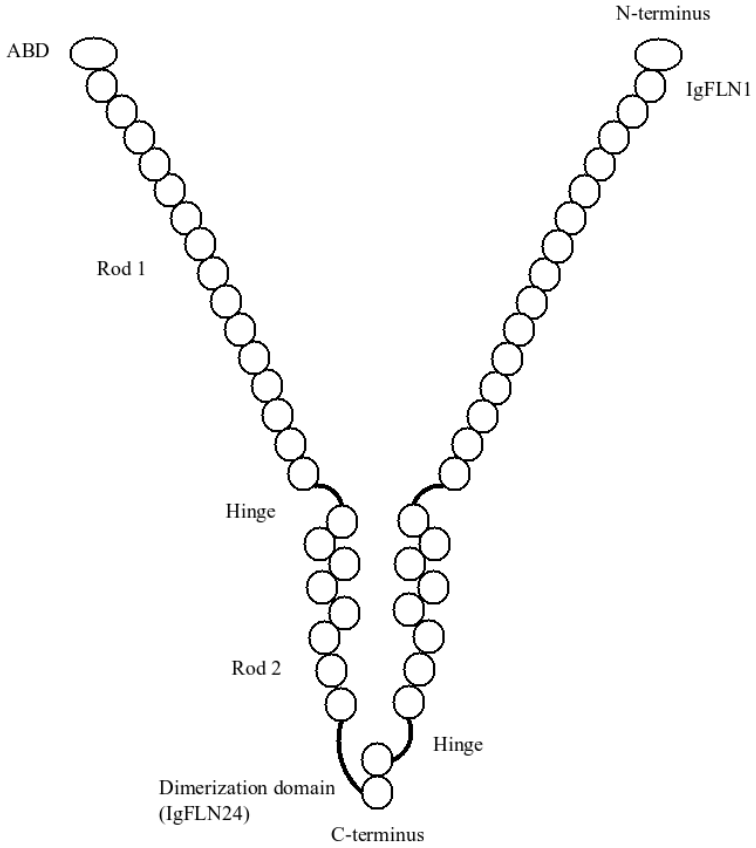

Figure 1: A schematic representation of mammalian FLNs. FLNs are V-shaped dimers consisting of an N-terminal ABD followed by a rod-like array of 24 Ig-like domains separated by two hinges. The most C-terminal domains mediate the dimerization.

The interactions of FLN ABD with actin and its regulation mechanisms are not fully understood (Nakamura et al., 2005). However, calmodulin, a Ca^{2+}-binding protein, inhibits FLNa binding to actin filaments. This interaction is not observed in the absence of actin filaments with complete FLN, but with denaturated ABD. Thus, calmodulin binds to cryptic sites in ABD. These results indicate that conformational changes in ABD occur upon binding to actin filaments (Nakamura et al., 2005).

Structure of immunoglobulin-like domains The structure of the repetitive domains of FLNs was first resolved from the *D. discoideum* FLN orthologue (Fucini et al., 1997). The domains are 100-residue β sandwich structures composed of two β sheets arranged into an Ig-like fold (figure 2B). The residues that form the core of the fold are conserved in human FLNs (Fucini et al., 1997). Excluding the two hinge regions, the linkers between the domains are relatively short and rich in proline. Occasionally salt bridges form between the two neighboring domains (for

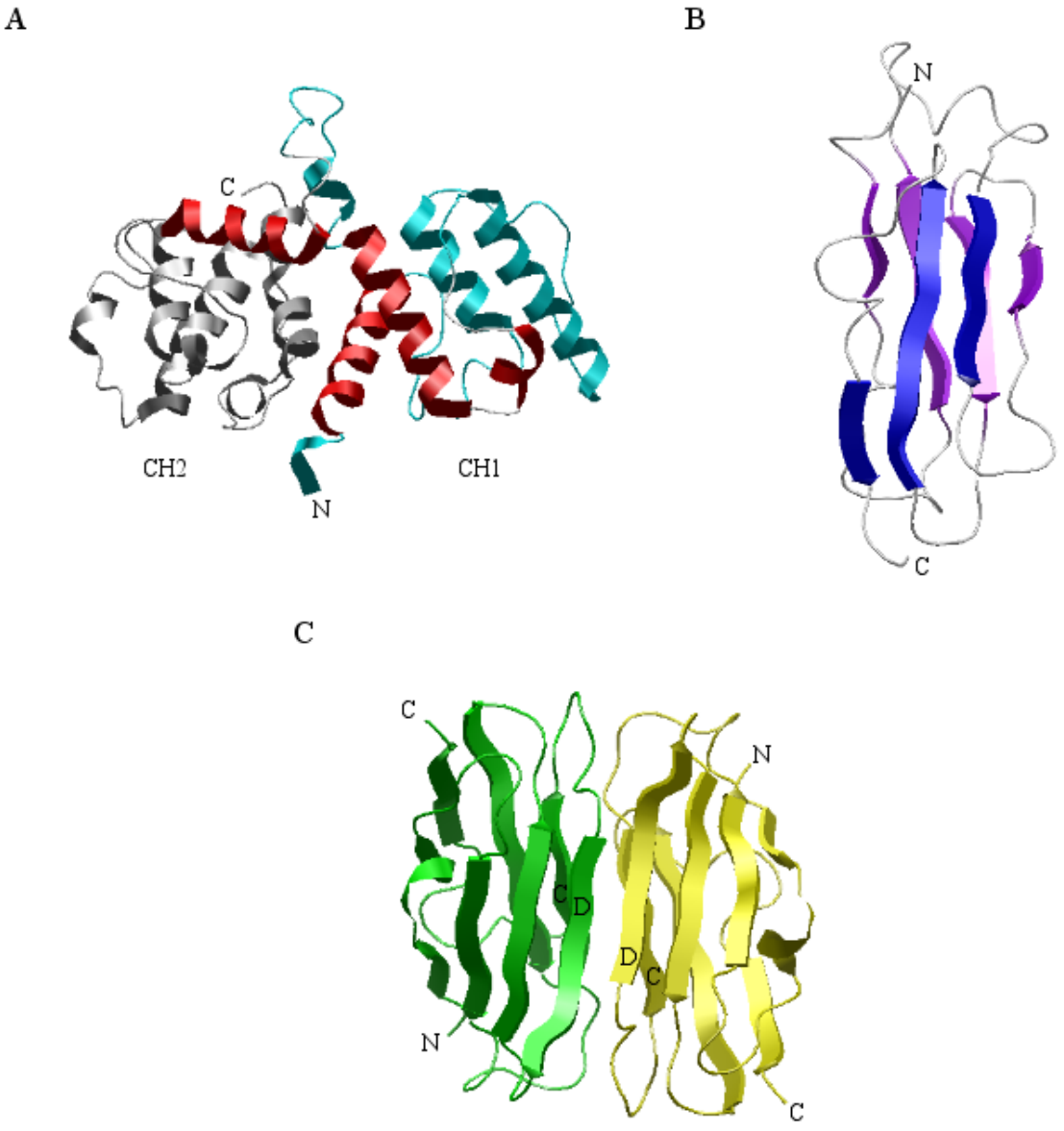

Figure 2: Structures of FLN domains. (A) Crystal structure of FLNa ABD (Brookhaven Protein Data Bank (PDB) code 3HOP, Clark et al., 2009). The ABD is consisted of two CH domains (CH1 and CH2) with three actin binding sequences. The CH1 domain is colored in light blue and the CH2 domain in gray. The actin binding sequences are colored in red. (B) Nuclear magnetic resonance structure of *D. discoideum* FLN rod domain four (PBD code 1KSR, Fucini et al., 1997). The domain is a β sandwich structure composed of two β sheets arranged into an Ig-like fold. The first β sheet is colored in magenta and the second in dark blue. (C) Crystal structure of IgFLNa24 dimer (PDB code 3CNK, Seo et al., 2008). The dimerization of FLN monomers is mediated by the hydrophobic interactions and hydrogen bonds between the two IgFLN24 domains. The domains are aligned antiparallel with respect to each other.

review see Popowicz et al., 2006).

Some of the domains in the rod two of FLNa form domain pairs (figure 3A). Nuclear magnetic resonance structure of IgFLNa18-19 (Heikkinen et al., 2009) and crystal structure of IgFLNa19-21 (Lad et al., 2007) show that the even numbered domains do not have complete Ig-like fold, but an unusual interaction with the following odd numbered domain. The A strands of domains 18 and 20 are folded along with the face formed by the C and D strands (CD face) of the domains 19 and 21, respectively. Furthermore, the order of the domains is not sequential – IgFLNa19 is followed by IgFLNa21 (Lad et al., 2007; Heikkinen et al., 2009). The solution structure of IgFLNa16-17 show also a pairwise folding of the domains, but as opposed to IgFLNa18-19 and 20-21, the A-strand of the domain 16 is not folded along with the domain 17, but is partly unstructured (Heikkinen et al., 2009). Structural characterization of IgFLNa18-21 based on small angle X-ray scattering (SAXS) data provides a model for the solution orientation of the four domain fragment (figure 3A) (Pentikäinen et al., 2010, manuscript). The domain pairs are arranged roughly perpendicularly to each other, and have very small interaction surface. This orientation differs slightly from that in the crystal structure of IgFLNa19-21. However, the crystallization may have influenced the conformation of the domains (Pentikäinen et al., 2010, manuscript). In line with this, molecular dynamics (MD) simulations have shown that IgFLNa19 and 20 can move in relation to each other (Lad et al., 2007).

Interestingly, the cryptic CD face of IgFLNa19 and 21 is a binding site for different proteins (table 1). Migfilin (Lad et al., 2008) as well as integrin β subunit cytoplasmic tails (Kiema et al., 2006) and glycoprotein Ibα (GPIbα) (Ithychanda et al., 2009B) bind preferentially to IgFLNa21 and more weakly to IgFLNa19. The crystal structure of IgFLNa21 in complex with integrin β7 cytoplasmic tail is shown in figure 4. The interaction is mediated via hydrophobic interactions and hydrogen bonds (Kiema et al., 2006). In fact, the CD faces of the IgFLN domains has been suggested to be a general ligand binding interface (Kiema et al., 2006). The interaction of GPIbα with IgFLNa17 (Nakamura et al., 2006) as well as migfilin with IgFLNa21 (Lad et al., 2008) are similar to integrin β7 binding. Several residues in the IgFLNa21 C strand that interact with integrin β7 are highly conserved in the C-terminal rod two odd-numbered domains. In contrast, the variability of the residues in the D strand could mediate the specificity of ligand binding (Kiema et al., 2006).

Structure of the dimerization domain Dimerization of the two FLN monomers is needed for FLN to be able to crosslink actin (Gorlin et al., 1990). The dimerization occurs non-covalently

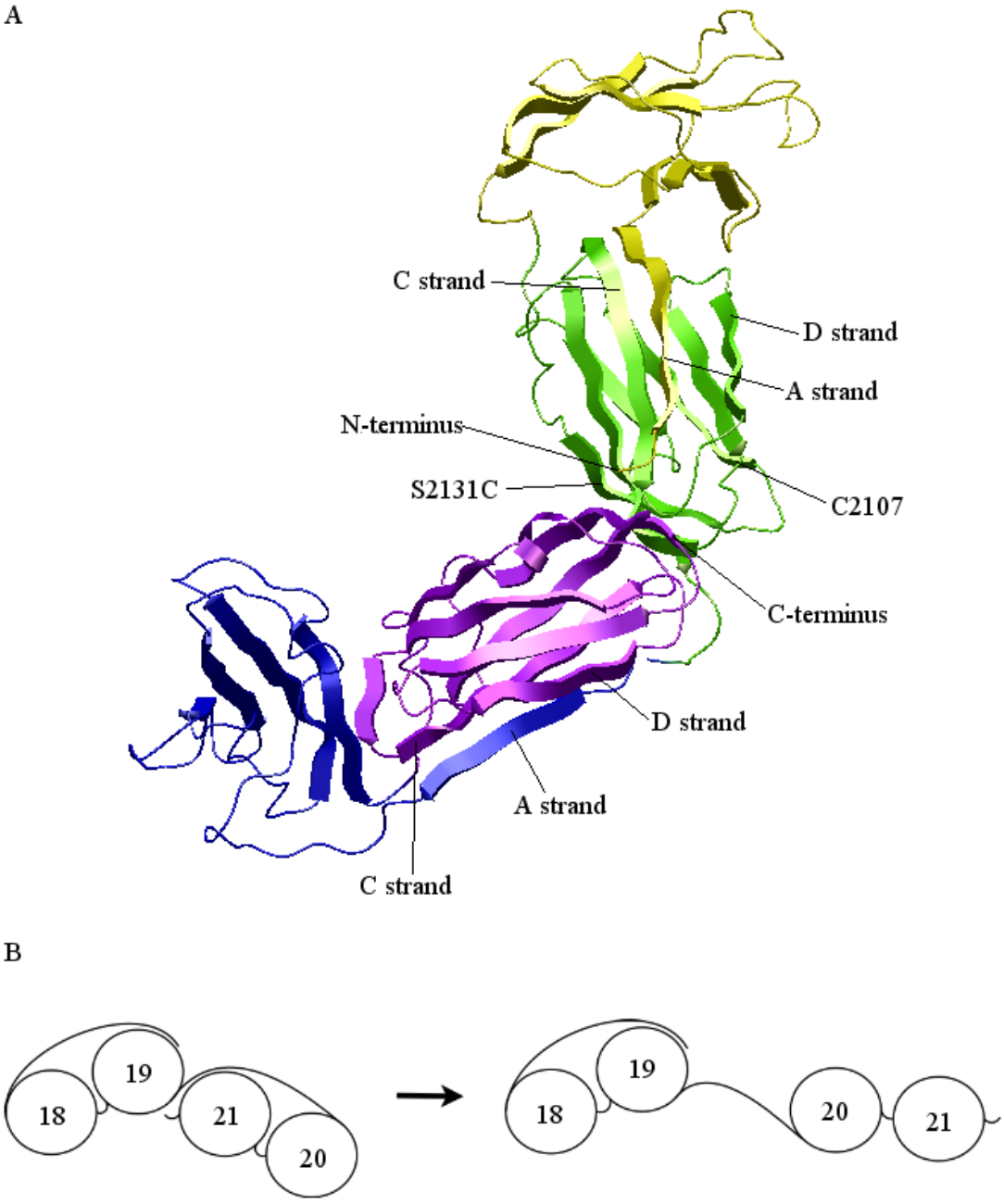

Figure 3: Structure of IgFLNa18-21. (A) Model structure of IgFLNa18-21 based on SAXS data (Pentikäinen et al., 2010, manuscript). IgFLNa18 is colored in yellow, IgFLNa19 in green, IgFLNa20 in blue, and IgFLNa21 in magenta. The domains are folded in a pairwise manner, where the A strands of the even numbered domains fold along with the CD face of the odd numbered domains. C2107 and S2131C represent the amino acids to which the fluorescent dye was attached. (B) A schematic representation of the hypothesized conformational change in the IgFLNa18-21 upon peptide binding. The peptide replaces the A strand of the IgFLNa20 masking the CD face of IgFLNa21 and makes the structure more flexible as the IgFLNa20-21 domain pair is free to swing along the replaced A strand.

via the most C-terminal domains (Seo et al., 2009). The crystal structures of human FLNa (Seo et al., 2009) and c (Pudas et al., 2005) have been determined, and their structures are almost identical (Seo et al., 2009). The dimerization domain is a β sandwich structure composed of two opposing β sheets. The dimerization occurs via the C and D strands of the domains. The domains are aligned antiparallel with respect to each other. Hydrophobic interactions as well as hydrogen bonds within the strands of the opposing domains mediate the dimerization (figure 2C) (Seo et al., 2009). The two-fold symmetry axis of the dimerization domains is aligned parallel to the long axis of the FLN dimer. This orientation allows the observed V-shaped structure of FLNs despite of the antiparallel arrangement of the dimerization domains (figure 1) (Pudas et al., 2005).

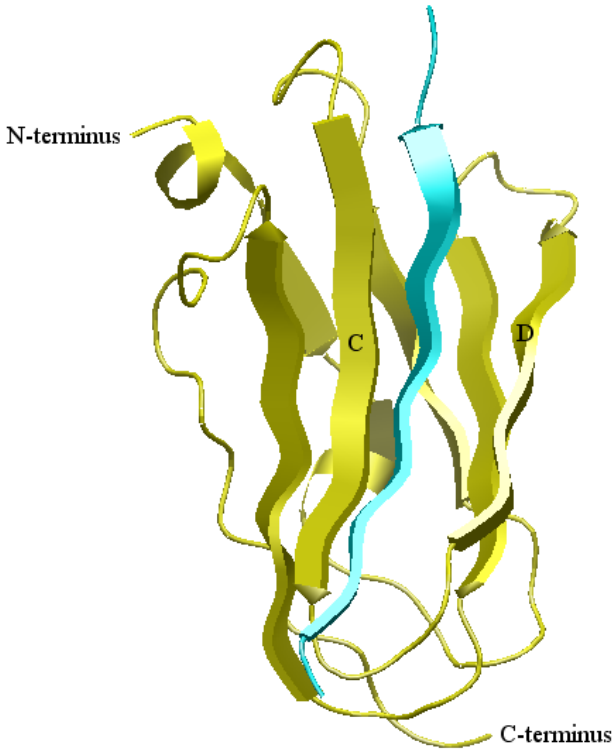

Figure 4: Crystal structure of IgFLNa21 in complex with integrin β7 (PDB code 2BRQ, Kiema et al., 2006). Integrin β7 (colored in light blue) binds to the CD face of IgFLNa21 (colored in yellow) via hydrophobic interactions and hydrogen bonds.

1.3 Biological functions of filamins

To date, FLNs have been shown to interact with plethora of proteins with diverse functions (for review see Zhou et al., 2007) of which examples are listed in table 1. The number of FLN interacting partners is yet increasing (for review see Zhou et al., 2010), and most likely important FLNb interacting partners remain to be identified as it is not as intensively studied as FLNa. Majority of the interacting partners bind to the C-terminal rod two domains while the N-terminal rod one domains mainly facilitate actin binding (for review see Zhou et al., 2010). Some of the biological functions of FLNs are discussed in more detail below.

Table 1: Examples of interacting partners of FLNs listed according to their functions. For more complete list see review Zhou et al., 2007. Many of the interactions presented here are discussed in more detail in the text.

isoform	interacting partners and their functions		interaction domain(s)	reference
FLNa	*adhesion*	Integrin β subunits	19, 21	for review see Zhou et al., 2010
		Migfilin	19, 21, 22	Lad et al., 2008
		GPIbα	17, 19, 21	Ithychanda et al., 2009B
	migration	Filgap [a)]	23	Nakamura et al., 2009
	signal transduction	RhoA, Rac1, Cdc42, RalA	24	Ohta et al., 1999
	kinase	p21-activated kinase 1	23	Vadlamudi et al., 2002
	transcription factor	Smad2 and 5	20-24	Sasaki et al., 2001
	protease	Calpains	hinge regions	Gorlin et al., 1990
	nuclear protein	Androgen receptor	16-19	Ozanne et al., 2002
		FOXC1	4-5, 6-9, 16-21	Berry et al., 2005
	tumour suppressor	BRCA-2	21-24	Yuan and Shen, 2001
	ion channels and cell surface receptors	Voltage-gated K^+ channel 4.2	not determined	Petrecca et al., 2000
		Dopamine receptors 2 and 3	16-19	Lin et al., 2001
	immunogenic function	Fc γ receptor I	not determined	Ohta et al., 1991
	vascular function	Tissue factor	24	Ott et al., 1998
		Calmodulin	ABD	Nakamura et al., 2005
	metabolic function	Insulin receptor	22-24	He et al., 2003
	FLN isoform	FLNb	24	Sheen et al., 2002
FLNb	*migration*	Migfilin	10-13	Takafuta et al., 2003
	transcription factor	Smad3	not determined	Zheng et al., 2007
	FLN isoform	FLNa	24	Sheen et al., 2002
FLNc	*signal transduction*	Protein kinase Bα	20	Murray et al., 2004
	protease	Calpain 3	hinge 1	Guyon et al., 2003
	muscle contraction	Sarcoglycans	not determined	Thompson et al., 2000

a) FLNa-binding RhoGTPase activating protein

1.3.1 Filamins in cell motility and adhesion

The migration of a cell needs controlled reorganization of the cytoskeleton and adhesion sites (for review see Ridley et al., 2003). Actin filaments produce the main protrusive force during cell migration via extensive polymerization at the leading edge of the polarized migrating cell (for review see Ridley et al., 2003). FLNs are needed to stabilize the network of actin filaments in migrating cells (Cunninham et al, 1992). The ability of FLNa-deficient cells to migrate is diminished due to improper polarization (Cunninham et al, 1992). FLNs have also been reported to regulate the initiation of migration and cell spreading (Baldassare et al., 2009). Knockout studies show that loss of single FLN isoform has little effect in migration but deficiency in FLNa and b or in all three isoforms impairs the initiation of migration and cell spreading, whereas re-expression of FLNa reverts them. These results also suggest a compensatory role for FLN isoforms (Baldassare et al., 2009).

Integrins are heterodimeric (α and β subunits) transmembrane adhesion molecules that bind into extracellular matrix via their N-terminal domains and into actin filaments via the C-terminal tail (for review see Hynes, 2002). This linkage enables signaling that is essential for cell survival, migration, and adhesion. Integrins exist in two conformations, inactive bent state and active open state (for review see Hynes, 2002). The activation is mediated by binding of talin into the cytoplasmic tail (Tadokoro et al., 2003). FLNs have been reported to bind several integrin β subunits (for review see Zhou et al., 2007) and their binding site overlaps with that of talin (Kiema et al., 2006) suggesting that competition of cytoplasmic protein binding is a regulatory mechanism in integrin activation. Thus, FLNs regulate processes dependent on integrin activation. For example, increased FLN binding to integrin inhibits cell migration (Calderwood et al., 2001).

Migfilin is a focal adhesion protein that participates in integrin mediated actin remodeling and cell shape modulation via FLN and kindlins (Tu et al., 2003). As already mentioned, migfilin binds to IgFLNa21 (Lad et al., 2008), and FLNs downregulate integrin activation (Calderwood et al., 2001). Interestingly, migfilin has higher affinity to FLNa than integrins (Ithychanda et al., 2009A). When binding to FLNa, migfilin dissociates FLNa from integrin promoting talin induced integrin activation. In addition, migfilin binds kindilin-2 and -3 and promotes their binding to integrin cytoplasmic tails. Kindlins regulate talin-mediated integrin activation (Ithychanda et al., 2009A). Thus, migfilin acts as a regulator of integrin activation (Lad et al., 2008).

1.3.2 Filamins in signal transduction and transcriptional regulation

FLNs contribute to the signal transduction by interacting with both cell surface receptors and intracellular signaling molecules. FLNs act as important scaffolds for intracellular signaling proteins involved in cell migration. FLNs bind to small GTPases, including Cdc42, RalA, Rac and Rho (Ohta et al., 1999) and several their up- and downstream effectors recruiting them to the vicinity of the plasma membrane of migrating cells (for review see Zhou et al., 2010). For example, RalA mediates filopodium formation via FLNa dependent manner (Ohta et al., 1999). Downstream from Rac, FLNa is needed in p21-activated kinase 1 controlled actin filament assembly (Vadlamudi et al., 2002). p21-activated kinase 1 is a Serine/Threonine kinase responsible for membrane ruffling (Vadlamudi et al., 2002). On the other hand, FLNa-binding RhoGTPase activating protein (filgap) specifically inactivates Rac and thereby suppresses leading edge protrusion and promotes cell retraction (Ohta et al., 2006). FLNs also anchor membrane receptors to actin cytoskeleton and contribute to their precise location in the cell membrane facilitating the downstream signaling pathways (for review see Zhou et al., 2007). Among other receptors, FLNa binds to the dopamine receptors 2 and 3, G-protein coupled central nervous system receptors (Lin et al., 2001) and to GPIbα, a receptor mediating signals leading to platelet activation (Feng et al., 2003).

FLNs act as both a positive and negative regulators of transcription. FLNa binds to p73a tumour suppressor and represses its transcriptional activity by preventing its nuclear localization (Kim et al., 2007). In addition, FLNa interacts with Smad2 and 5 promoting their phosphorylation and subsequent nuclear localization and activation (Sasaki et al., 2001). However, FLNb represses the phosphorylation of Smad3 (Zheng et al., 2007). These results indicate distinct functions for FLN isoforms in the regulation of transcription. Smad transcription factors interact with transforming growth factor β superfamily receptors mediating signals that regulate organ development and homeostasis (Sasaki et al., 2001). FLNs regulate transcription also by directly interacting with nuclear proteins. FLNa interacts with BRCA-2, a tumour suppressor that has a role in the repair of damaged DNA (Yuan and Shen 2001). In addition, FLNa inhibits the function of FOXC1 in the nucleus (Berry et al., 2005). FLNa binds to PBX1 transcription regulator and carries it into the nucleus where it forms a transcription-inhibitory complex with FOXC1. FOX transcription factors regulate the organ development during embryogenesis (Berry et al., 2005). Furthermore, a calpain-cleaved fragmented FLNa promotes the nuclear localization of androgen receptor (Ozanne et al., 2000). Androgen receptor regulates the development of male phenotype (Ozanne et al., 2000). FLNa represses the transactivation of androgen receptor and

disrupts its interdomain interactions, thus promoting its down-regulation (Loy et al., 2003).

1.4 Regulation of filamin associated interactions

Competition of ligand binding provides a regulatory mechanism for FLN mediated interactions. As previously mentioned, the overlapping binding sites for talin, integrin β subunit cytoplasmic tails (Kiema et al., 2006) and migfilin (Lad et al., 2008; Ithychanda et al., 2009A) suggest that FLNs negatively regulate the integrin activation by competing with talin on binding to integrins, whereas migfilin promotes integrin activation upon binding to FLNs, thus allowing talin binding to integrins. Furthermore, immunoglobulin binding to Fc gamma receptor I, a receptor involved in antibody-mediated immune responses, decreases the interaction of the receptor with FLNa that functions as an anchor for the receptor and links it to the actin cytoskeleton (Ohta et al., 1991). Release of the receptor from FLNa leads to reorganization of actin cytoskeleton (Ohta et al., 1991).

Masking of the ligand binding sites suggests an autoinhibitory mechanism of ligand binding in FLNa (Lad et al., 2007). The CD faces of IgFLNa19 and 21 form the ligand binding sites and are masked by the A strand of the preceding domains (figure 3A) (Lad et al., 2007; Heikkinen et al., 2009; Pentikäinen et al., 2010 manuscript). The deletion of the masking A strand from the preceding domains increases integrin β7 binding as well as do point mutations that weaken the A strand interactions with the CD face (Lad et al., 2007). Furthermore, integrin binding is significantly stronger with the single domains IgFLNa19 and 21, respectively.

The diversity of FLNs is increased by alternative splicing (for review see Zhou et al., 2010). For example, alternative splicing of FLNs regulates integrin binding (van der Flier et al., 2002). Splice variants of FLNa and FLNb that lack amino acids from the IgFLN19-20 region have been shown to have higher affinity to integrin β subunits than the wild-type isoforms. This is likely the result of the exposure of cryptic binding sites (van der Flier et al., 2002). Interestingly, the expression of FLN splice variants differs according to tissue and cell location indicating delicate specialized functions for different splice variants (for review see Zhou et al., 2009).

As the ligand binding CD faces in IgFLNa19 and 21 are masked by the A strand of the preceding domains, the exposure requires a significant change in the protein conformation (Lad et al., 2007). Steered MD simulations made with IgFLNa18-19, 20-21, and 19-21 structures show that induced mechanical force exposes the cryptic binding sites in IgFLNa19 and 21 in

a sequential manner (Pentikäinen and Ylänne, 2009). The conformation of the CD face is not altered by the induced force. These results indicate a mechanotransductory role for FLNs as the force-induced conformational change allows ligand binding (Pentikäinen and Ylänne, 2009). In addition, atomic force microscopy studies made with human FLNa (Furuike et al., 2001) and *D. discoideum* FLN (Schwaiger et al., 2004) show that the mechanical stress induced unfolding of the Ig-like domains is reversible. The unfolded domains gradually refold as the applied force is reduced near to zero. These results suggest that the repetitive domains of FLNs may serve as a mechanically extensible elements that help for instance in the stabilization of cell shape against small stress (Furuike et al., 2001; Schwaiger et al., 2004).

FLNs are subjected to proteolysis by various proteases which alter their biological functions (for review see van der Flier and Sonnenberg, 2001). For instance, the proteolytic cleavage with calpain produces two asymmetric heavy and light filamin fragments and disrupts the ability of FLNa to crosslink actin (Davies et al., 1978) In addition, calpain cleaved fragmented FLNa represses the activity of androgen receptor (Ozanne et al., 2000), as already mentioned. The proteolysis is believed to be regulated by phosphorylation and, indeed, phosphorylation reduces susceptibility of FLNs to calpain cleavage (for review see van der Flier and Sonnenberg, 2001). All FLN isoforms contain a conserved cAMP kinase consensus site that makes them resistant to calpain cleavage when phosphorylated (for review see van der Flier and Sonnenberg, 2001).

Phosphorylation also affects the binding capacity of FLNs (for review see van der Flier and Sonnenberg, 2001). Protein kinases that phosphorylate FLNs include cAMP-kinase, PKC and Ca^{2+}/calmodulin dependent protein kinase II, among others (for review see van der Flier and Sonnenberg, 2001). For instance, the ability of FLNa to crosslink actin is increased upon Ca^{2+}/calmodulin dependent protein kinase II phosphorylation (Ohta and Hartwig, 1995). Moreover, a mutation to aspartic acid that mimics serine phosphorylation in one dopamine receptor 2 phosphorylation site diminishes FLN binding (Li et al., 2000) showing that also phosphorylation of FLN interacting proteins has a regulatory effect on FLNs.

1.5 Filamin associated diseases

As described earlier, FLNs have been shown to have distinct functions besides their main role as actin crosslinking proteins. Mutations in FLN genes cause several abnormalities, some of them lethal, showing an important role of FLNs during the development. Recently, mouse models of deficiency for all three FLN isoforms have been reported (for review see Zhou et al., 2010).

Depletion of any of the three FLN isoforms is lethal and is therefore likely to be so in humans as well. Different mutations lead to similar phenotypes as seen in human disorders, which bring more detailed information to the molecular mechanisms behind them (for review see Zhou et al., 2010).

1.5.1 Filamin A defects

Periventricular nodular heterotopia is an FLNA associated brain malformation disorder where neurons fail to migrate into the cerebral cortex. This result in clusters of neurons in lateral ventricle where the neurons are generated (Fox et al., 1998). The disorder is caused by several nonsense and frameshift mutations in the FLNA gene, thus leading to loss of function (for review see Robertson, 2005). Majority of the males die during the embryogenesis or neonatally for extensive hemorrhage (Eksioglu et al., 1996). Majority of the patients are heterozygous females that have normal intelligence but suffer from epileptic seizures and malformations in digestive and respiratory organs. The defects are thought to be caused by mosaic X chromosome inactivation (Eksioglu et al., 1996; Fox et al., 1998).

Otopalatodigital syndrome, frontometaphyseal dysplasia and Melnick Needles syndrome cause a skeletal dysplasia and abnormalities in intestinal and reproductive organs as well as heart defects. These disorders are caused by various missense or in-frame deletions in FLNA (for review see Robertson, 2005). In addition, missense mutations in FLNA cause X-linked myxoid valvular dystrophy, characteristic of valvular diseases and anomalies such as mitral valve prolapse (Kyndt et al., 2007).

1.5.2 Filamin B and C defects

Mutations in FLNB cause several skeletal disorders that disrupt skeletogenesis, joint formation, vertebral segmentation and ossification of limbs and vertebrae. Nonsense mutations in FLNB that result in truncated FLNb or loss of function cause autosomal recessive spondylocarpotarsal syndrome (Krakow et al., 2004). Missense mutations in FLNB cause autosomal dominant atelosteogenesis (types I and III), Larsen syndrome and, perinatally lethal boomerang dysplasia (Bicknell et al., 2005). A nonsense mutation in FLNC result in an unfolded dimerization domain incapable of forming dimers. This leads to autosomal dominant myofibrillar my-

opathy – a progressive weakening of skeletal muscles due to cytoplasmic aggregates of FLNc and other muscle cell related proteins (Vorgerd et al., 2005).

1.6 Förster resonance energy transfer

Förster resonance energy transfer (FRET) is an increasingly popular method among biologists to study for instance protein-protein interactions in cells and conformational changes of proteins. The theory for resonance energy transfer was developed by physicist Theodor Förster in the 1940's after whom the phenomena has been named (Lakowicz, 2006).

In FRET, energy from an excited fluorophore, in this case called a donor, is non-radiatively transferred to another molecule, an acceptor, through long-range dipole-dipole interactions (Lakowicz, 2006). For this to occur, the emission spectrum of the donor must overlap with the absorption spectrum of the acceptor. FRET experiments are typically conducted with two fluorophores. The acceptor however does not need to be fluorescent. FRET occurs only between molecules that are sufficiently close to each other, typically within 1-10 nm range. FRET occurs always when the donor and acceptor come into distance that allows energy transfer (Lakowicz, 2006).

The energy transfer efficiency (E), i.e. the FRET efficiency, measures the fraction of photons absorbed by the donor that are transferred to the acceptor, and is defined by equation (1)

$$E = \frac{R_0^6}{R_0^6 + r^6}, \tag{1}$$

where r is the distance of the donor and acceptor and R_0 is the Förster radius, i.e. the distance where 50% of FRET occurs – the other half of the excitation energy is dissipated by other processes, such as emission or heat. Thus, the energy transfer efficiency is strongly dependent on the distance of the molecules. This result in sharp increase or decrease in the energy transfer efficiency as the distance separating the molecules becomes greater or minor than R_0 (figure 5). Consequently, for distances close to R_0 FRET can be used as a molecular ruler for determining distances of the molecules. It is important to remember that when measuring changes in distances, the result is a scalar and thus does not tell which of the molecules move (Lakowicz, 2006).

The Förster radius R_0 is unique for every FRET pair and is defined by equation (2)

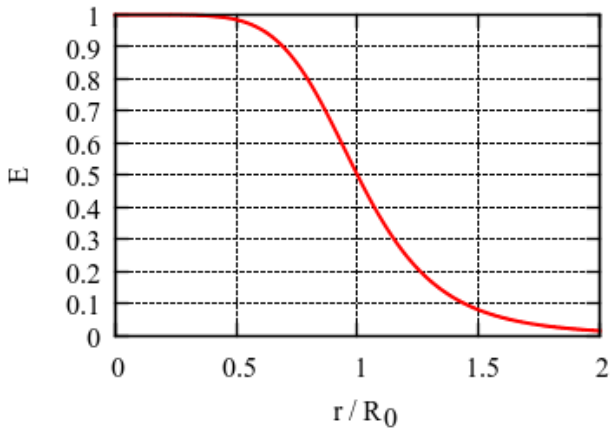

Figure 5: Dependence of the energy transfer efficiency (E) on the distance separating the donor and acceptor (r). The Förster radius R_0 is the distance where 50% of FRET occurs. Because of strong dependence on the distance according to equation (1), the curve has a sharp fall-off.

$$R_0 = \left[2.8 * 10^{17} * \kappa^2 * Q_D * \varepsilon_A * J(\lambda)\right]^{\frac{1}{6}}, \tag{2}$$

where κ^2 is the angle between the donor and acceptor transition dipoles, Q_D is the donor quantum yield, i.e. the efficiency of the fluorescence, ε_A is the maximal acceptor extinction coefficient, and $J(\lambda)$ is the spectral overlap integral between the normalized donor fluorescence $F_D(\lambda)$ and acceptor excitation $E_A(\lambda)$ spectra

$$J(\lambda) = \int F_D(\lambda) * F_A(\lambda) * \lambda^4 d\lambda. \tag{3}$$

For maximum FRET to occur, the donor and acceptor transition dipole orientations need to be approximately parallel to each other. The κ^2 is usually assumed to be 2/3 which is the average value integrated over all possible angles (Lakowicz, 2006).

The energy transfer efficiency can be calculated according to equation (4) from the relative fluorescence intensity of the donor in the absence (F_D) and presence (F_{DA}) of the acceptor or from the fluorescence lifetime, i.e. the average time the fluorophore stays in the excited state, under respective conditions (τ_D and τ_{DA})

$$E = 1 - \frac{F_{DA}}{F_D} = 1 - \frac{\tau_{DA}}{\tau_D}. \tag{4}$$

This equation is applicable only in situations where the donor and acceptor are separated by a

fixed distance, such as in double-labeled proteins (Lakowicz, 2006).

The equation (1) shown above can further be simplified to give

$$< r >= R_0 \left(\frac{1}{E} - 1 \right)^{\frac{1}{6}}, \tag{5}$$

from which the average distance of the donor and acceptor can be calculated using the FRET efficiency (Lakowicz, 2006).

A major source of error in calculating the distances from the FRET efficiencies rises from the incomplete labeling with the acceptor (Lakowicz, 2006). Molecules not labeled with the donor do not contribute to the donor emission intensity and can thus be neglected, assuming that the extent of donor labeling is the same for donor only and donor-acceptor pair. If the fractional labeling f_A is known, equation (4) can be modified to calculate the energy transfer efficiency in 1:1 stoichiometric labeling situation of donor and acceptor (Lacowicz, 2006)

$$E = 1 - \frac{F_{DA} - F_D(1 - f_A)}{F_D f_A} = \left(1 - \frac{F_{DA}}{F_D} \right) \frac{1}{f_A} = \left(1 - \frac{\tau_{DA}}{\tau_D} \right) \frac{1}{f_A}. \tag{6}$$

2 Aim of the study

Recent study provides a solution model for IgFLNa18-21 based on SAXS data (figure 3A) (Pentikäinen et al., 2010 manuscript). The study shows that IgFLNa18-21 changes its conformation upon binding to an interacting partner. This was studied with full-length IgFLNa18-21 and a splice variant that lacks the last β strand of IgFLNa19 and the first β strand (A strand) of IgFLNa20 which masks the ligand binding CD face of IgFLNa21. The maximum dimensions of the protein predicted by SAXS data increased upon migfilin binding in the full-length IgFLNa18-21, but not in the splice variant. These results suggest that migfilin binding replaces the masking A strand of IgFLNa20 and induces a conformational change leading to a flexibilization of the structure as IgFLNa20-21 is free to swing along the A strand (figure 3B) (Pentikäinen et al., 2010 manuscript). The aim of this study was to demonstrate this conformational change using FRET.

3 Materials and methods

3.1 Mutagenesis and cloning

FLNA18-21 pGEX-4T3 TEV plasmid was mutated with QuickChange Lightning Multi Site-directed Mutagenesis Kit (Agilent Technologies) to produce a unique site for a thiol reactive fluorophore conjugation. Two variants, one containing five mutations (named C2107 after the fluorophore conjugation site) and other containing seven mutations (named S2132C) were produced. The mutations and their sites along with the corresponding mutagenesis primers (Oligomer) are listed in table 2. The mutated constructs were purified with QIAPrep Spin Miniprep and QIAQuick PCR Purification Kits (Qiagen) and subsequently sequenced with ABI3130 DNA Sequencer (Applied Biosystems) using BigDye Terminator Sequencing Kit (Applied Biosystems).

Table 2: Mutagenesis primers. Listed are also the mutated amino acids and their respective domains. The mutated codon is marked on bold text in the primer. Primers marked in italics were used to produce the variant containing five mutations. All primers but the second (C2102S only) were used to produce the other variant.

domain	mutation	primer
18	*C1997S*	*5' CGG GAG GAG CCC **TCT** TTG CTG AAG CGG CTG 3'*
19	*C2102S*	*5' GAG GAC GGG ACG **TCC** AGG GTC ACC TAC TGC 3'*
19	C2102S, C2107S	5' G GAC GGG ACG **TCC** AGG GTC ACC TAC **TCC** CCC ACA GAG C 3'
19	S2131C	5' CCT GGC AGC CCC TTC **TGT** GTG AAG GTG ACA GGC 3'
20	*C2160S*	*5' GCC AAC GTT GGT AGT CAT **TCT** GAC CTC AGC CTG 3'*
20	*C2199S*	*5' GAG AAC CAC ACC TAC **TCC** ATC CGC TTT GTT CCC 3'*
21	*C2293S*	*5' CGC AAG GAC GGC TCC **TCT** GGT GTG GTC TAT GTG 3'*

A fusion protein containing enhanced green fluorescent protein (EGFP) in the C-terminus of mutated FLNA18-21 linked with a recognition sequence for PreScission protease was produced with sequential PCRs using Phusion High-Fidelity Polymerase (Finnzymes). First, BbsI-FLNA18- 21-PreScission and PreScission-EGFP-NotI (from pEGFP-N1, Clontech) fragments were generated and purified from 1% agarose gel (Promega) with GeneCleanII Kit (Qbiogene). These fragments served as annealing templates to produce the fusion protein construct using forward primer from the FLNA18-21 fragment reaction and reverse primer from the EGFP fragment reaction. The primers (Oligomer) are listed in table 3.

The FLNA18-21-EGFP constructs and pGEX-4T3- TEV plasmid were digested with BbsI and NotI restriction enzymes (New England Biolabs) and ligated with T4 ligase (New England Biolabs). The FLNA1821-EGFP pGEX-4T3 TEV was transformed into Inoue Ultracompetent

Table 3: Primers for the ligation of FLNA18-21 and EGFP with sequential PCR.

fragment	primer
FLNA forward	5' TAT AGA AGA CAA CAT GTC CAT GCG TAT GTC CCA CCT AAA GG 3'
FLNA reverse	5' GGG CCC CTG GAA CAG AAC TTC CAG ACC AGA CGG AGA AGC CAC AGG C 3'
EGFP forward	5' CTG GAA GTT CTG TTC CAG GGG CCC ATG GTG AGC AAG GGC GAG GAG 3'
EGFP reverse	5' TAT AGC GGC CGC TTA CTT GTA CAG CTC GTC CAT GCC G 3'

Escherichia coli DH5α cells. The constructs were purified and sequenced as described above.

3.2 Protein expression and purification

The FLNA18-21-EGFP pGEX-T3 TEV were transformed into Inoue Ultracompetent *E. coli* BL21-GOLD cells. The cells were grown in lysogeny broth with 200 µg/ml ampicillin (AppliChem) and protein expression was induced with 0.4 µM IPTG (Fermentas) when A_{600} of the cell cultures reached 0.6. The proteins were expressed for overnight incubation at +26°C. Cell cultures were then centrifuged (6079 x *g*) for 15 min at +4°C and resuspended into PBS.

The cells were disrupted with French Press Cell Pressure (Thermo Scientific) at 2000 PSI. 1% (v/v) Triton X-100 (Prolabo) was added to lysate and incubated at +4°C for 30 min. The proteins were then purified with Glutathione Sepharose 4 Fast Flow affinity chromatography (GE Healthcare). GST was digested on the column with Tobacco etch virus protease for overnight at +4°C after which the proteins were eluted in 20 mM Tris, 100 mM NaCl pH=8.00. The proteins were further purified with gel filtration (ÄKTA Prime Plus, column HiLoad 26/20 Superdex 75, Amersham Biosciences) and eluted in 20 mM Tris, 100 mM NaCl pH=7.00. The proteins were concentrated to approximately 1 mg/ml.

3.3 Fluorophore labeling

10 times molar excess of Alexa Fluor 532 C_5-maleimide (Invitrogen) diluted in DMSO was added in drops to the protein solution and incubated for 2 h at room temperature in slow rotation and subsequently dialyzed vigorously overnight at +4°C against 20 mM Tris, 100 mM NaCl pH=7.00. All steps were carried out protected from light. The degree of labeling was calculated using the equation (7) (from Invitrogen)

$$mol_{dye}/mol_{protein} = \left(\frac{A}{\varepsilon}\right)\left(\frac{M}{c}\right) \tag{7}$$

where A is the absorption and ε molar extinction coefficient of the dye at the absorption maximum, and M the molecular mass and c the concentration (in mg/ml) of the protein.

3.4 Steady-state and time-resolved fluorescence measurements

Steady-state fluorescence spectra were measured with Perkin Elmer LS55 Luminescence spectrometer. Excitation wavelengths of 488 nm and 535 nm were used. Time-resolved fluorescence measurements were carried out using a homemade time-correlated single photon counting system with HydraHarp 400 photon counting instrumentation and software from PicoQuant. Excitation wavelength of 485 nm was used and emission was collected using filter with central wavelength of 498 nm and full width at half maximum of 10.9 nm. The intensity decay data were analyzed using a multiexponential fluorescence decay fitting

$$I_t = \sum_i^n A_i exp(-t/\tau_i) \tag{8}$$

where A_i is the amplitude of a component ($\sum A_i = 1$), τ_i its fluorescence lifetime and n the number of decay times. The analysis was made with a home-made program. The best-fit parameters were obtained by minimization of the reduced χ^2 value. The average FRET efficiency was calculated according to equation (6) using the average donor fluorescence lifetime in the absence $<\tau_D>$ and presence $<\tau_{DA}>$ of the acceptor. The average fluorescence lifetime was calculated by summing up the fluorescence lifetimes of individual components multiplied with their respective amplitudes

$$<\tau>=\sum_i A_i\tau_i\,. \tag{9}$$

The Förster distance R_0 for EGFP-Alexa Fluor 532 C_5-maleimide FRET-pair was calculated with FRETView program (Stevens et al., 2007). The transition dipole orientation factor was assumed to be 2/3 and refractive index of the buffer 1.33.

The protein solution had $A_{488} \approx 0.1$ in all samples. Samples were measured before and after pep-

tide addition. 10 or 100 times molar excess of peptide was used in the measurements. The following custom peptides (EZBiolab) were used: migfilin (residues 5-19 and 5-28), ^{5}PEKRVASSV FITLAP^{19}PRRDVAVAE^{28}; integrin β7 (residues 771-788), QDSNPLYKSAITTTINP; GPIbα (residues 557-579), RGSLPTFRSSLFLWVRPNGRVPL and filgap (residues 723-736), EQFFS TFGELTVEP.

3.5 Molecular dynamics simulations

The atomic coordinates for IgFLNa18-21 were taken from the model based on SAXS data (Pentikäinen et al., 2010 manuscript) and for EGFP from crystal structure of GFP (PDB code 1EMA, Yang et al., 1996). The linker having a recognition sequence for PreScission protease between IgFLNa18-21 and GFP was built with Jackal nest package (Xiang, 2002). The intrinsic fluorophore of GFP was mutated *in silico* to natural amino acids. Leap module of AmberTools 1.4 (Schafmeister et al., 1995) was used to solvate the protein construct into a box of water molecules with appropriate number of sodium ions to neutralize the system. The starting structures were modified and molecular dynamics (MD) simulation structure figures were made with Bodil (Lehtonen et al., 2004). Trajectory analysis were performed with ptraj6.5 (stand-alone version online[1]).

MD simulations and energy minimizations were done with NAMD 2.4 (Phillips et al., 2005) using Amber ff03 force field parameters (Duan et al., 2003) and TIP3P model (Jorgensen et al., 1983) for water molecules. System relaxation and equilibration was done as follows: [1] water molecules and counter ions were minimized with the deepest-descent algorithm (3000 steps) keeping rest of the system fixed. [2] Similar minimization as above restraining only the C^{α} atoms to their initial positions with harmonic force of 5 $kcal/mol/\AA^2$. [3] MD simulation at constant volume for 300 ps and [4] at constant pressure for further 300 ps for the whole system C^{α} atoms fixed. [5] Finally, MD simulation for the whole system at constant pressure without any restrictions for 8.65 ns was performed. Calculated root-mean-square deviations (RMSDs) showed that the system was equilibrated.

The system was kept at a constant temperature of 300 K using Langevin dynamics for nonhydrogen atoms, with a Langevin damping coefficient of 5 ps^{-1}. A constant pressure of 1 atm was maintained using the Langevin piston method (Feller et al., 1995). An oscillation timescale of

[1] available: http://www.chpc.utah.edu/~cheatham/software.html

200 fs and a damping timescale of 100 fs were used. Equilibration phase simulations were performed with an integration time step of 2 fs under a multiple-time-stepping scheme (Schlick et al., 1999). Bonded and short-range interactions were computed every time step and long-range electrostatic interactions every third step. A cutoff of 12 Å was used for van der Waals and short-range electrostatic interactions. To ensure a smooth cutoff, a switching function was started at 10 Å for the van der Waals interactions. Long-range electrostatic interactions were calculated using particle mesh Ewald method (Darden et al., 1993; Essmann et al., 1995; Sagui and Darden, 1999; Toukmaji et al., 2000). SHAKE algorithm was used to constrain bonds containing hydrogen atoms (Ryckaert et al., 1977).

4 Results

4.1 Protein purification and fluorophore labeling

First, FLNA18-21 was mutated to produce a unique site for fluorophore labeling. Two different mutants were produced (figure 3A). Second, EGFP was cloned to the C-terminus of FLNA18-21, and the recombinant plasmid FLNA18-21-EGFP pGEX-T3 TEV was constructed. Then, the recombinant fusion protein was expressed by IPTG induction and subsequently purified with affinity chromatography and gel filtration. First of all, the solubility of FLNa18-21-EGFP was low, thereby the purification process needed to be optimized. In addition, the cleavage of the GST tag was incomplete which further complicated the purification. However, pure protein was recovered after final purification step (figure 6A and B) albeit low amount, less than 3 mg out of 6-8 l cell cultures. Not all of the uncleaved protein was separated during the gel filtration which further lowered the recovery. Also, there were some minor impurities of unknown lower molecular weight protein. The chromatograms for the gel filtration of both constructs are in appendix I.

Purified FLNa18-21-EGFP was labeled with thiol reactive Alexa Fluor 532 C_5 maleimide to produce a FRET pair. The degree of labeling was calculated according to equation (7). The degree of labeling for C2107 and S2131C, respectively, were 0.61 and 0.55. Thus, slightly over half of the proteins were labeled. The absorption spectra of the proteins are shown in figure 6C. The absorption peak of the acceptor was near 530 nm and at slightly different positions in both constructs.

4.2 The effect of peptide addition to donor fluorescence emission

A conformational change in IgFLNa18-21 upon peptide addition was studied using FRET. Three peptides with different affinities to FLNa18-21 were used. Filgap binds to IgFLNa23 (Nakamura et al., 2009) and was used as a negative control. First, steady-state fluorescence was used to measure the amount of energy transfer before and after peptide addition. Excitation wavelengths near the absorption maximum of the donor (488 nm) and the acceptor (535 nm) were used. No exact values for energy transfer efficiency were calculated.

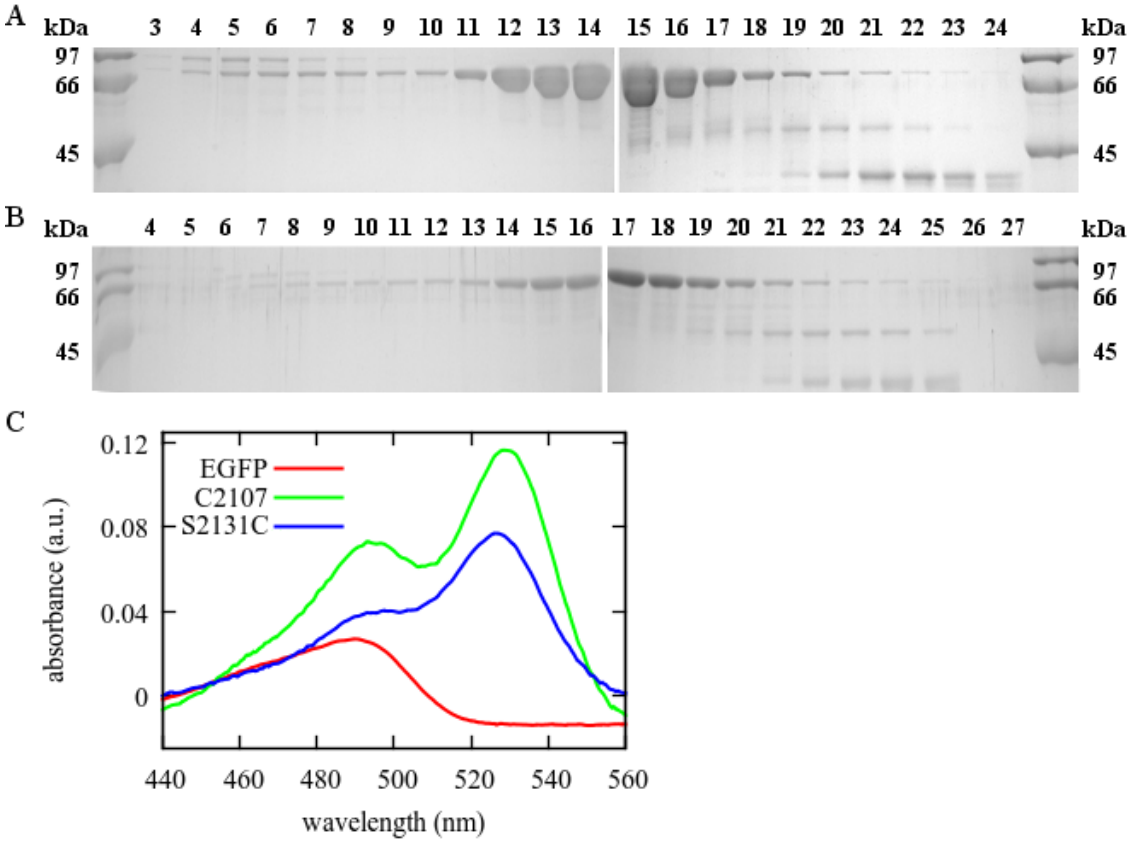

Figure 6: Purification and fluorophore labeling of FLNa18-21-EGFP. (A-B) SDS-PAGE of the gel filtration of (A) C2107 and (B) S2131C. Analyzed fractions are marked with running numbering. Not all of the uncleaved protein (approximately 98 kDa) was separated from the cleaved protein (approximately 73 kDa) which lowered the recovery. Fractions 11-15 of C2107 and 9-17 of S2131C contained the pure FLNa18-21-EGFP and were combined. The gel filtration chromatograms are shown in appendix I. (C) The absorption spectra of the purified and acceptor labeled proteins. The spectra are normalized to the same protein concentration (A_{280}).

In figure 7 are shown the emission spectra obtained from the steady-state fluorescence measurements. Measurements with migfilin peptide were repeated with both constructs giving similar results. FRET was observed clearly as the intensity of the donor emission decreased in comparison to control that was labeled only with the donor EGFP. Part of the excitation energy was transferred to the acceptor, forming the peak nearer the red end of the spectrum. No notable change was observed in the energy transfer efficiency after peptide addition. Only GPIbα and migfilin (10 times molar excess) addition induced modest increase in the donor emission in C2107. Furthermore, addition of migfilin in C2107 (100 times molar excess) and in S2131C (10 times molar excess) led to decrease in the donor emission suggesting aggregation. In addition, the acceptor was quenched upon peptide addition. This is clearly seen as a decrease in the acceptor emission. Filgap addition resulted neither acceptor quenching nor a change in energy transfer efficiency.

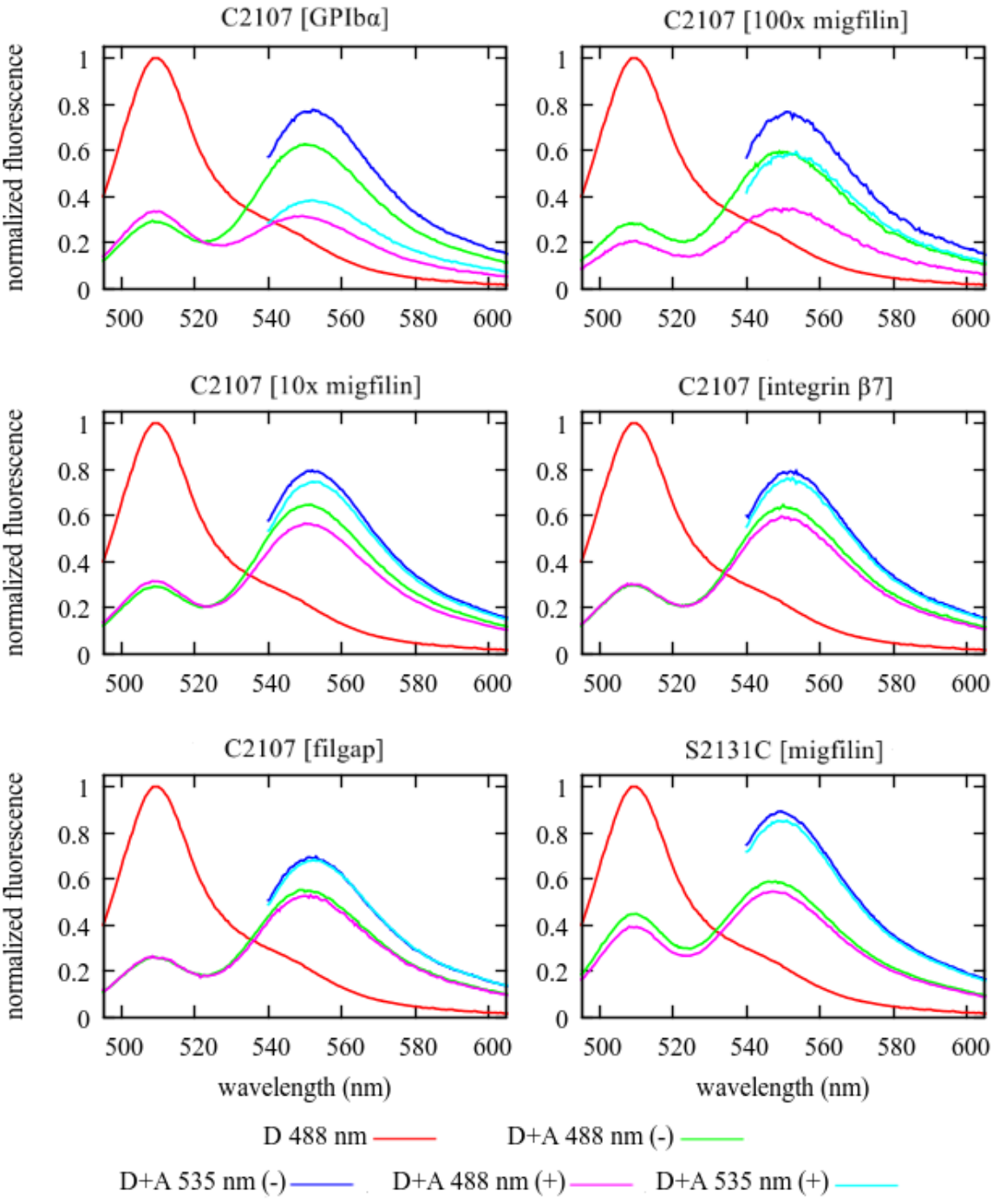

Figure 7: Steady-state fluorescence spectra. Shown here are the relative fluorescence emission of C2107 and S2131C with respect to donor emission before (-) and after (+) peptide addition. Excitation wavelengths near the absorption maximum of the donor [D] (488 nm) and acceptor [A] (535 nm) were used. Migfilin peptide was added both 100 and 10 times molar excess and all other peptides 10 times molar excess. Filgap was used as a negative control. Measurements with migfilin peptide were repeated giving similar results.

4.3 The effect of peptide addition to donor fluorescence lifetime

The effect of peptide addition to the amount of energy transfer was further examined with time-resolved fluorescence measurements. The parameters acquired from all the measurements are listed in table 4. The fluorescence decay curves before peptide addition for control (donor only) and for C2107 and S2131C in comparison to control with respective best fits and residuals are shown in figure 8. The decay curves after peptide addition are essentially the same and are not shown for clarity. The decay curve becomes steeper as the amount of energy transfer increases showing greater efficiency for C2107 than for S2131C. The average fluorescence lifetimes (<τ>) of the donor were calculated from the decay parameters according to equation (9) and are shown in table 4. The average lifetimes before and after peptide addition, respectively, calculated for all measurements (excluding negative control) were 1.86 ±0.10 ns and 1.91 ±0.10 ns for C2107 and 2.55 ±0.10 ns and 2.48 ±0.10 ns for S2131C. Thus, no statistically significant difference in the fluorescence lifetime was detected after peptide addition in either constructs. Moreover, after GPIbα and migfilin (100 times molar excess) addition, visible aggregation occurred.

The average lifetimes were used to calculate energy transfer efficiencies (E) and average distances of the fluorophores (<r>) for each measurement. The calculated values are listed in table 4. The average distance of the fluorophores for all measurements, before and after peptide addition, respectively, were 5.17 ±0.59 nm and 5.27 ±0.71 nm for C2107 and 6.72 ±2.13 nm and 6.50 ±1.43 nm for S2131C.

4.4 Molecular dynamics simulation structure of FLNa18-21-EGFP

Finally, MD simulations were run to analyze the stability of the protein construct and the orientation of the EGFP fusion partner. The RMSD analysis showed that the construct was stable and did not lead to unfolding (figure 9B) as the deviation of the structure with respect to the initial structure did not increase recklessly, but showed steady increase. The EGFP was located at the convex side of the L-shaped IgFLNa18-21 (figure 9A). The simulation showed only modest movement of the EGFP in relation to IgFLNa18-21.

The distance of the fluorophores was estimated from one of the structures obtained from the MD simulations. The distance was calculated between the EGFP center of mass and the C^{α} of the amino acids to which the acceptor fluorophore was conjugated. In figure 9C is shown the distance over the whole simulation time with both constructs. The average distance calculated

Table 4: The decay parameters for the time-resolved fluorescence measurements. The fluorescence decay of the donor was measured in the absence and presence of the acceptor. In the presence of the acceptor the decay was measured before (-) and after (+) peptide addition. The intensity decay data were analyzed according to equation (8) using the multiexponential fluorescence decay fitting. First, the average lifetimes (<τ>) were calculated from the decay parameters according to equation (9). Then, the average lifetimes were used to calculate the energy transfer efficiencies (E) and subsequently the average distances of the fluorophores (<r>) according to equations (6) and (5), respectively. Thus, the fractional labeling of the proteins with the acceptor has been taken into account in the calculation of (E). The error in <τ> is simply the range of the data set.

sample	peptide		χ^2	A_1	A_2	τ_1 (ns)	τ_2 (ns)	$<\tau>$ (ns)	E	$<r>$ (nm)
Donor only			229.438	1.00	-	2.92 ±0.01	-	2.92 ±0.01	-	-
C2107	GPIbα	-	295.432	0.62	0.38	2.45 ±0.05	0.79 ±0.04	1.82 ±0.09	0.62 ±0.11	5.09 ±0.43
		+	265.260	0.65	0.35	2.36 ±0.02	0.60 ±0.04	1.74 ±0.06 *	0.66 ±0.07	4.94 ±0.51
	migfilin5-28 (100x)	-	263.210	0.69	0.31	2.41 ±0.04	1.00 ±0.03	1.85 ±0.07	0.60 ±0.09	5.16 ±0.65
		+	297.675	0.73	0.27	2.44 ±0.03	0.86 ±0.03	1.95 ±0.06 *	0.54 ±0.07	5.37 ±0.52
	migfilin5-28	-	131.452	0.70	0.30	2.42 ±0.04	0.80 ±0.06	1.93 ±0.10	0.56 ±0.12	5.30 ±0.49
		+	203.711	0.64	0.36	2.53 ±0.03	0.86 ±0.04	1.92 ±0.07	0.56 ±0.09	5.30 ±0.72
		-	254.975	0.65	0.35	2.45 ±0.03	0.80 ±0.04	1.87 ±0.07	0.59 ±0.09	5.20 ±0.65
		+	237.163	0.66	0.34	2.56 ±0.05	0.94 ±0.06	2.00 ±0.11	0.52 ±0.13	5.45 ±0.97
	migfilin5-19	-	288.343	0.64	0.36	2.44 ±0.04	0.80 ±0.04	1.85 ±0.08	0.60 ±0.09	5.16 ±0.65
		+	271.325	0.68	0.32	2.51 ±0.05	0.90 ±0.05	1.98 ±0.10	0.53 ±0.12	5.41 ±0.89
	integrinβ7	-	201.475	0.64	0.36	2.44 ±0.03	0.76 ±0.04	1.83 ±0.07	0.61 ±0.09	5.12 ±0.65
		+	183.759	0.66	0.34	2.43 ±0.03	0.76 ±0.05	1.86 ±0.08	0.60 ±0.09	5.16 ±0.65
	filgap	-	245.324	0.64	0.36	2.44 ±0.03	0.76 ±0.04	1.84 ±0.07	0.61 ±0.09	5.12 ±0.65
		+	229.450	0.65	0.35	2.44 ±0.04	0.77 ±0.05	1.86 ±0.09	0.60 ±0.11	5.16 ±0.08
S2131C	migfilin5-28	-	267.267	0.84	0.16	2.80 ±0.06	1.11 ±0.05	2.54 ±0.11	0.24 ±0.15	6.69 ±2.17
		+	239.008	0.84	0.16	2.74 ±0.03	0.82 ±0.06	2.42 ±0.09	0.31 ±0.12	6.31 ±1.24
		-	267.296	0.84	0.16	2.82 ±0.06	1.12 ±0.04	2.55 ±0.10	0.23 ±0.14	6.75 ±2.09
		+	253.477	0.86	0.14	2.78 ±0.04	0.95 ±0.05	2.53 ±0.09	0.24 ±0.12	6.69 ±1.62

* Small amount of aggregation was observed at the bottom of cuvette after the measurement.

from the trajectory data for C2107 and S2131C were 5.23 nm and 6.49 nm, respectively.

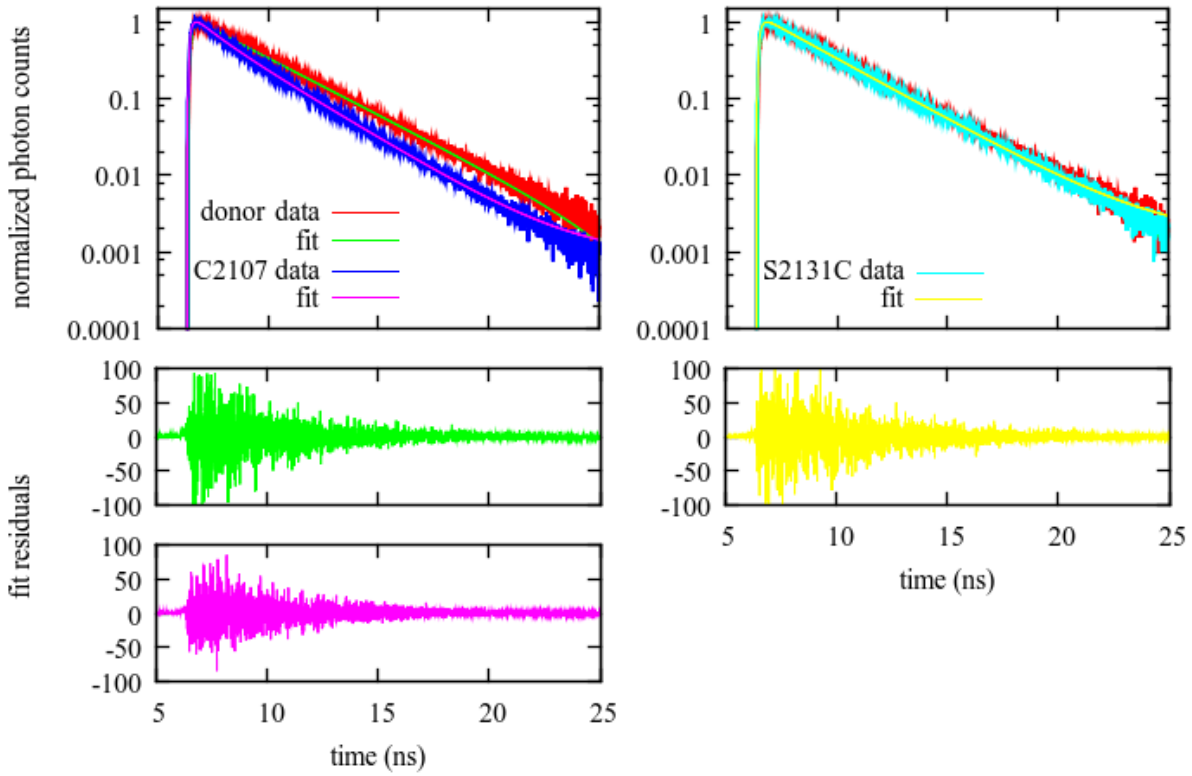

Figure 8: The normalized fluorescence intensity decay curves for C2107 and S2131C in comparison to the donor EGFP only. Shown here are also the best multiexponential decay fits and respective residuals. The intensity decay for C2107 and S2131C was measured before and after peptide addition. Only the decay curves before peptide addition are shown for clarity – the decay curves after peptide addition are essentially the same. The decay parameters for all measurements are listed in table 4.

5 Discussion

The aim of the study was to determine a conformational change in FLNa18-21 upon ligand addition. It has been shown that applied force exposes the masked ligand binding sites, the CD faces, of IgFLNa19 and 21 (Pentikäinen and Ylänne, 2009). This is thought to serve as a regulatory mechanism for binding of integrins and other interacting partners to FLNa (Pentikäinen and Ylänne, 2009). However, recent study implies that no applied force is needed, but migfilin binds to IgFNa21 without prior replacement of the masking A strand of the preceding domain inducing a major conformational change in IgFLNa20-21 (figure 3B) (Pentikäinen et al., 2010, manuscript). This conformational change was studied here using FRET.

EGFP was cloned to the C-terminus of FLNa18-21 which was first mutated to have a unique site for acceptor fluorophore conjugation to produce a FRET pair. Two different mutants were produced (figure 3A). Finally, the fusion proteins were purified with chromatographic methods. However, the EGFP lowered the solubility of the proteins substantially which complicated the purification and resulted in low protein recovery. A thiol reactive Alexa Fluor 532 C_5 maleimide was used as an acceptor. The fluorophore labeling was successful and the fluorophore pair formed overlapping absorption spectra forming a FRET pair (figure 6C). The acceptor fluorophore had absorption maximum near 530 nm and at slightly different positions with both constructs. The conjugation resulted in minor blue shift of the fluorophore (absorption maximum at 532 nm according to the manufacturer) slightly increasing its spectral overlap with the donor EGFP.

Interestingly, EGFP has one cysteine relatively close to the surface to which the fluorophore may conjugate (figure 9A). In such a case, the proteins used in the measurements could be double-labeled or also mixtures of proteins that have a label in two different conjugation sites. The degree of labeling to these sites cannot be controlled, but it is likely that the energy transfer efficiencies for both constructs would be close to each other if such mixed labeling had occurred. This however was not observed, as will be discussed in more detail below.

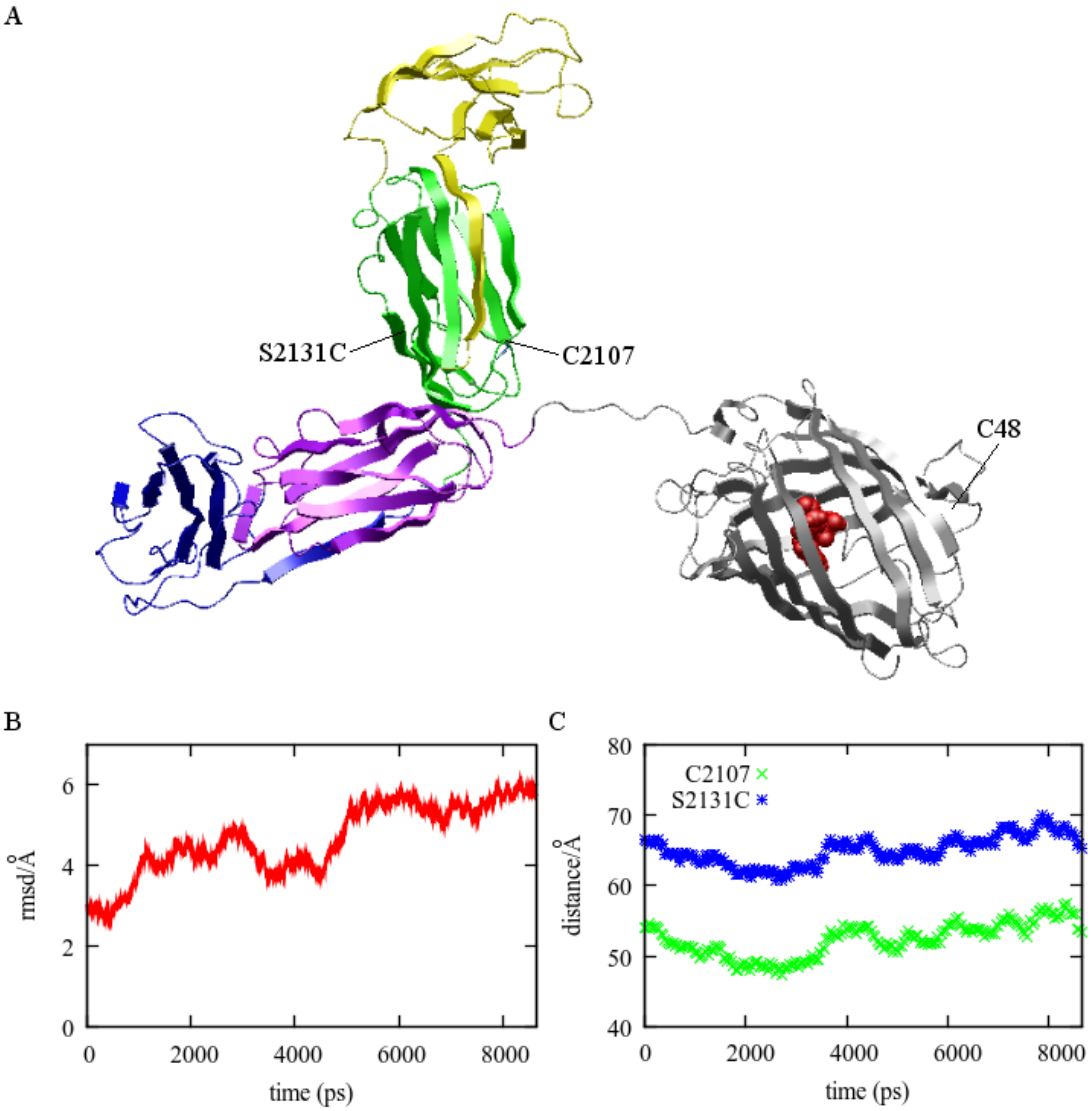

Figure 9: MD simulations. (A) MD simulation structure of IgFLNa18-21-EGFP. IgFLNa18 is colored in yellow, IgFLNa19 in green, IgFLNa20 in blue, IgFLNa21 in magenta, and EGFP in gray. The EGFP was oriented at the convex side of IgFLNa18-21. The simulation showed only modest movement of the EGFP in relation to IgFLNa18-21. C48 represents the cysteine residue near the surface of the EGFP. (B) The RMSD analysis for IgFLNa18-21-EGFP. (C) The distance of the intrinsic fluorophore of EGFP (colored in red) and the site of acceptor fluorophore conjugation for C2107 and S2131C.

5.1 Peptide addition did not change the amount of energy transfer

The effect of peptide addition to the amount of energy transfer was first studied with steady-state fluorescence. Any exact values for energy transfer efficiency to be compared with the time-resolved measurements were not calculated. This would have required the use of several

correction factors, all of which were not taken into consideration during the measurements (for review see Wouters et al., 2001). There was practically no change in the amount of energy transfer before and after peptide addition (figure 7). Only a modest increase in the fluorescence intensity of the donor was observed upon GPIbα and migfilin addition. However, in these cases, the decrease in the acceptor fluorescence intensity could not be determined because of quenching interactions. Thus, according to the results, no clear change in the conformation of IgFLNa18-21 occurred. As mentioned, the acceptor was quenched upon peptide addition. The quenching was strongest upon GPIbα addition and weakest upon integrin addition. Filgap, that was used as a negative control, did not result in notable quenching. Interestingly, GPIbα has highest affinity to IgFLNa21 and integrin the lowest (Ithychanda et al, 2009B). Thus, the higher affinity the used peptide has to IgFLNa21 the higher quenching resulted.

Alexa fluorophores are quenched by certain natural amino acids, including tryptophan, tyrosine, histidine and methionine (Chen et al., 2010). However, the used peptides do not contain these amino acids as only GPIbα has one tryptophan, so direct evidence for the quenching interactions of the peptides with the fluorophore cannot be addressed. Another explanation could be that peptide binding induces a conformational change in IgFLNa18-21 that influences the near environment of the fluorophore. This is well in line with the fact that filgap addition did not induce notable quenching of the acceptor (figure 7). Filgap binds to IgFLNa23, but not to IgFLNa19 or -21 (Nakamura et al., 2009). All the other peptides that were used bind preferentially to IgFLNa21, but also to IgFLNa19 (Kiema et al., 2006; Lad et al., 2008; Ithychanda et al., 2009B). The acceptor fluorophore was attached into two sites (C2107 and S2131C, respectively) in IgFLNa19 close to IgFLNa21 (figure 3A). These sites are relatively near the CD face of IgFLNa19. Peptide binding to IgFLNa19 could explain the observed quenching as the peptide replaces the A strand masking the CD face, thus inducing conformational changes of the protein in the near environment of the fluorophore. Fluorescent properties of fluorophores are affected by environmental influences (for review see Wouters et al., 2001).

The effect of peptide addition to the amount of energy transfer was further examined with time-resolved fluorescence measurements. The data obtained (table 4 and figure 8) is well in line with the steady-state fluorescence data. The average fluorescence lifetime of the donor calculated for all measurements (excluding the negative control) before and after peptide addition, respectively, were 1.86 $\pm$0.10 ns and 1.91 $\pm$0.10 ns for C2107 and 2.55 $\pm$0.10 ns and 2.48 $\pm$0.10 ns for S2131C. Consequently, no statistically meaningful change in the fluorescence lifetime was observed upon peptide addition. A notable decrease in the fluorescence intensity of the donor was observed after addition of 100 times molar excess of migfilin to C2107 (figure

7). In addition, aggregate was observed at the bottom of the cuvette after time-resolved fluorescence measurements. Small decrease in the donor fluorescence intensity was observed in both measurements with S2131C and 10 times molar excess of migfilin (figure 7). However, no aggregation was observed. Nevertheless, these results imply that the peptide addition led to minor aggregation of the proteins. This was not surprising because of already low solubility of the proteins. Taken together, no significant change in the energy transfer was detected with either constructs indicating that no major conformational change occurred or that the used method simply was not sensitive for the possible conformational change. The two constructs had significantly different energy transfer efficiencies. Also, peptide addition led to aggregation of the protein.

5.2 Distance calculations give insight to the orientation of the domain pairs

The stability of the protein construct and especially the orientation of the EGFP fusion partner was analyzed in more detail with MD simulations. The RMSD analysis (figure 9B) showed that the construct was stable. The EGFP was oriented at the convex side of the L-shaped IgFLNa18-21 (figure 9A). The simulation showed only modest movement of EGFP in relation to IgFLNa18-21. However, the simulation time was short and given indefinitely time the EGFP would probably move more since there are no apparent disruptive interactions. It is reasonable to assume that the EGFP would nevertheless be oriented at the convex side of IgFLNa18-21 rather than at the concave side due to steric hindrances.

The original reason to attach the acceptor fluorophore to two distinct sites in IgFLNa19 was to obtain information about the orientation of the domain pairs IgFLNa18-19 and 20-21 within each other. The solution model for IgFLNa18-21 is based on SAXS data (Pentikäinen et al., 2010, manuscript) and the resolution of SAXS is not sufficient to indicate the exact orientation of the domain pairs within each other. The average distance of the donor and acceptor fluorophores was calculated both from the trajectories obtained from MD simulations data (figure 9C) and the time-resolved fluorescence data (table 4). The average distances obtained from the trajectories were 5.23 nm and 6.49 nm for C2107 and S2131C, respectively. The average distances calculated for all measurements from the time-resolved fluorescence data, before and after peptide addition, respectively, were 5.17 $\pm$0.59 nm and 5.27 $\pm$0.71 nm for C2107 and 6.72 $\pm$2.13 nm and 6.50 $\pm$1.43 nm for S2131C. The intermolecular FRET was not taken into consid-

eration which results in overestimation of the energy transfer efficiencies from which the average distances were calculated. However, the average distances obtained from the time-resolved fluorescence data are reasonably well in line with the ones obtained from the MD simulations trajectories. Thus, based on the average distances obtained in this study the C2107 is indeed oriented closer to the donor fluorophore as in the SAXS structure used in the MD simulations (Pentikäinen et al., 2010, manuscript) (figure 9C and D).

5.3 Future perspectives

The conformational change in IgFLNa20-21 upon peptide binding was not observed in this study. Suppose that the binding site masking A strand balance between bound and unbound state, peptide addition would have led to lesser change in the energy transfer as the binding sites are only partly uncrypted. Nevertheless, the change in energy transfer should have been detectable as excess of peptide drives the balancing reaction to unbound state.

It is also unclear whether the EGFP in the C-terminus of IgFLNa18-21 had a disruptive effect on the dynamics of the structure. GFP has a tendency to produce dimers in solution via hydrophobic interactions (Yang et al., 1996), and the results imply that peptide addition led to aggregation of the protein. These events could further disrupt the dynamics as several proteins are packed in proximity. In such a case, one possibility would be to replace the EGFP with synthetic organic fluorophore. However, as seen in this study and as demonstrated with other Alexa dyes (Chen et al., 2010), the quenching interactions of the fluorophores and the protein to which they are conjugated forms a major problem regarding the use of FRET. Considering this, the use of fluorescent proteins is supported by the fact that their intrinsic fluorophore is well protected from any disruptive interactions (Yang et al., 1996). Still, changes in the construct are needed in further experiments to increase the solubility of the protein and to reduce any possible disruptive interactions of the EGFP. For instance, the length of the IgFLNa constructs could be revisited as well as the possibility to link fluorescent protein to the N-terminus of IgFLNa. Also, the acceptor fluorophore conjugation site could be located further away from the peptide binding CD face.

As already discussed, peptide binding to IgFLNa19 could explain the observed quenching of the acceptor fluorophore by influencing the near environment of the fluorophore. Preferential binding of the peptides to IgFLNa19 instead of IgFLNa21 could also explain why no change in the energy transfer efficiencies was detected in this study. Peptide binding to IgFLNa19 does

not induce major conformational change that would be detected with the used constructs. The binding to IgFLNa21 could be disrupted or completely abolished because of the EGFP. Further experiments are required to verify this. One option would be to introduce mutations that disrupt binding to IgFLNa19 and mutations that promote binding to IgFLNa21.

More extensive use of controls would improve the interpretation of the results. In addition to control that is labeled with only the donor, a control labeled with only the acceptor should be used. In this case the amount of intermolecular FRET could be estimated by mixing these uni-labeled controls into the same sample. Furthermore, the effect of peptide to fluorescence emission properties of the donor and acceptor, respectively, could be defined by adding peptide to each control sample. In these experiments, the effect of peptide addition to fluorescence emission of the donor EGFP could not be determined.

In conclusion, the conformational change in IgFLNa18-21 could not be determined. The reason remains unclear, though it is possible that the EGFP disrupted the dynamics of IgFLNa18-21 or that the peptide binding to IgFLNa21 was disrupted. Also, the solubility of the proteins was low and peptide addition led to aggregation of the proteins. However, it is also possible that the used method was not sensitive for the possible conformational change in this construct in which case alternative methods should be considered. All in all, changes in the construct are needed in further experiments, should FRET be used. Finally, the two constructs used had significantly different energy transfer efficiency values which can be used to deduct the orientation of the domain pairs IgFLNa18-19 and 20-21.

References

Baldassarre, M., Z. Razinia, C.F. Burande, I. Lamsoul, P.G. Lutz, and D.A. Calderwood. 2009. *Filamins regulate cell spreading and initiation of cell migration*. PLoS One. 4:e7830.

Berry, F.B., M.A. O'Neill, M. Coca-Prados, and M.A. Walter. 2005. *FOXC1 transcriptional regulatory activity is impaired by PBX1 in a filamin A-mediated manner*. Mol.Cell.Biol. 25:1415-1424.

Bicknell, L.S., T. Morgan, L. Bonafe, M.W. Wessels, M.G. Bialer, P.J. Willems, D.H. Cohn, D. Krakow, and S.P. Robertson. 2005. *Mutations in FLNB cause boomerang dysplasia*. J.Med.Genet. 42:e43.

Calderwood, D.A., A. Huttenlocher, W.B. Kiosses, D.M. Rose, D.G. Woodside, M.A. Schwartz, and M.H. Ginsberg. 2001. Increased filamin binding to beta-integrin cytoplasmic domains inhibits cell migration. Nat.Cell Biol. 3:1060-1068.

Chen, H., S.S. Ahsan, M.B. Santiago-Berrios, H.D. Abruna, and W.W. Webb. 2010. *Mechanisms of quenching of Alexa fluorophores by natural amino acids*. J.Am.Chem.Soc. 132:7244-7245.

Clark, A.R., G.M. Sawyer, S.P. Robertson, and A.J. Sutherland-Smith. 2009. *Skeletal dysplasias due to filamin A mutations result from a gain-of-function mechanism distinct from allelic neurological disorders*. Hum.Mol.Genet. 18:4791-4800.

Cunningham, C.C., J.B. Gorlin, D.J. Kwiatkowski, J.H. Hartwig, P.A. Janmey, H.R. Byers, and T.P. Stossel. 1992. *Actin-binding protein requirement for cortical stability and efficient locomotion*. Science. 255:325-327.

Darden, T., D. York, and L. Pedersen. 1993. *Partile mesh Ewald: an N [center-dot] log(N) method for Ewald sums in large systems.* J.Chem.Phys. 98:10089-10092.

Davies, P.J., D. Wallach, M.C. Willingham, I. Pastan, M. Yamaguchi, and R.M. Robson. 1978. *Filamin-actin interaction. Dissociation of binding from gelation by Ca^{2+}-activated proteolysis*. J.Biol.Chem. 253:4036-4042.

Eksioglu, Y.Z., I.E. Scheffer, P. Cardenas, J. Knoll, F. DiMario, G. Ramsby, M. Berg, K. Kamuro, S.F. Berkovic, G.M. Duyk, J. Parisi, P.R. Huttenlocher, and C.A. Walsh. 1996. *Periventricular heterotopia: an X-linked dominant epilepsy locus causing aberrant cerebral cortical development*. Neuron. 16:77-87.

Essmann, U., L. Perera, M.L. Berkowitz, T. Darden, H. Lee, and L.G. Pedersen. 1995. *A smooth particle mesh Ewald method.* J.Chem.Phys. 103:8577-8593.

Etienne-Manneville, S., and A. Hall. 2002. *Rho GTPases in cell biology*. Nature. 420:629-635.

Feller, S.E., Y. Zhang, R.W. Pastor, and B.R. Brooks. 1995. *Constant pressure molecular dynamics simulation: the Langevin piston method*. J.Chem.Phys. 103:4613-4621.

Feng, S., J.C. Resendiz, X. Lu, and M.H. Kroll. 2003. *Filamin A binding to the cytoplasmic tail of glycoprotein Ibalpha regulates von Willebrand factor-induced platelet activation*. Blood. 102:2122-2129.

Fox, J.W., E.D. Lamperti, Y.Z. Eksioglu, S.E. Hong, Y. Feng, D.A. Graham, I.E. Scheffer, W.B. Dobyns, B.A. Hirsch, R.A. Radtke, S.F. Berkovic, P.R. Huttenlocher, and C.A. Walsh. 1998. *Mutations in filamin 1 prevent migration of cerebral cortical neurons in human periventricular heterotopia*. Neuron. 21:1315-1325.

Fucini, P., C. Renner, C. Herberhold, A.A. Noegel, and T.A. Holak. 1997. *The repeating segments of the F-actin crosslinking gelation factor (ABP-120) have an immunoglobulin-like fold*. Nat.Struct.Biol. 4:223-230.

Furuike, S., T. Ito, and M. Yamazaki. 2001. *Mechanical unfolding of single filamin A (ABP-280) molecules detected by atomic force microscopy*. FEBS Lett. 498:72-75.

Gorlin, J.B., R. Yamin, S. Egan, M. Stewart, T.P. Stossel, D.J. Kwiatkowski, and J.H. Hartwig. 1990. *Human endothelial actin-binding protein (ABP-280, nonmuscle filamin): a molecular leaf spring*. J.Cell Biol. 111:1089-1105.

Guyon, J.R., E. Kudryashova, A. Potts, I. Dalkilic, M.A. Brosius, T.G. Thompson, J.S. Beckmann, L.M. Kunkel, and M.J. Spencer. 2003. *Calpain 3 cleaves filamin C and regulates its ability to interact with gamma- and delta-sarcoglycans*. Muscle Nerve. 28:472-83.

He, H.J., S. Kole, Y.K. Kwon, M.T. Crow, and M. Bernier. 2003. *Interaction of filamin A with the insulin receptor alters insulin-dependent activation of the mitogen-activated protein kinase pathway*. J.Biol.Chem. 278:27096-27104.

Heikkinen, O.K., S. Ruskamo, P.V. Konarev, D.I. Svergun, T. Iivanainen, S.M. Heikkinen, P. Permi, H. Koskela, I. Kilpeläinen, and J. Ylänne. 2009. *Atomic structures of two novel immunoglobulin-like domain pairs in the actin crosslinking protein filamin*. J.Biol.Chem. 284:25450-25458.

Hynes, R.O. 2002. *Integrins: bidirectional, allosteric signaling machines*. Cell. 110:673-687.

Ithychanda, S.S., M. Das, Y.Q. Ma, K. Ding, X. Wang, S. Gupta, C. Wu, E.F. Plow, and J. Qin. 2009A. *Migfilin, a molecular swhich in regulation of integrin activation*. J.Biol.Chem. 284:4713-4722.

Ithychanda, S.S., D. Hsu, H. Li, L. Yan, D.D. Liu, M. Das, E.F. Plow, and J. Qin. 2009B. *Identification and characterization of multiple similar ligand-binding repeats in filamin: implication on filamin-mediated receptor clustering and cross-talk*. J.Biol.Chem. 284:35113-35121.

Kiema, T., Y. Lad, P. Jiang, C.L. Oxley, M. Baldassarre, K.L. Wegener, I.D. Campbell, J. Ylänne, and D.A. Calderwood. 2006. *The molecular basis of filamin binding to integrins and competition with talin*. Mol.Cell. 21:337-347.

Kim, E.J., J.S. Park, and S.J. Um. 2007. *Filamin A negatively regulates the transcriptional activity of p73alpha in the cytoplasm*. Biochem.Biophys.Res.Commun. 362:1101-1106.

Korenbaum, E., and F. Rivero. 2002. *Calponin homology domains at a glance*. J.Cell.Sci. 115:3543-3545.

Krakow, D., S.P. Robertson, L.M. King, T. Morgan, E.T. Sebald, C. Bertolotto, S. Wachsmann-Hogiu, D. Acuna, S.S. Shapiro, T. Takafuta, S. Aftimos, C.A. Kim, H. Firth, C.E. Steiner, V. Cormier-Daire, A. Superti-Furga, L. Bonafe, J.M. Graham Jr, A. Grix, C.A. Bacino, J. Allanson, M.G. Bialer, R.S. Lachman, D.L. Rimoin, and D.H. Cohn. 2004. *Mutations in the gene encoding filamin B disrupt vertebral segmentation, joint formation and skeletogenesis*. Nat.Genet. 36:405-410.

Kyndt, F., J.P. Gueffet, V. Probst, P. Jaafar, A. Legendre, F. Le Bouffant, C. Toquet, E. Roy, L. McGregor, S.A. Lynch, R. Newbury-Ecob, V. Tran, I. Young, J.N. Trochu, H. Le Marec, and J.J. Schott. 2007. *Mutations in the gene encoding filamin A as a cause for familial cardiac valvular dystrophy*. Circulation. 115:40-49.

Lad, Y., P. Jiang, S. Ruskamo, D.S. Harburger, J. Ylänne, I.D. Campbell, and D.A. Calderwood. 2008. *Structural basis of the migfilin-filamin interaction and competition with integrin beta tails*. J.Biol.Chem. 283:35154-35163.

Lad, Y., T. Kiema, P. Jiang, O.T. Pentikäinen, C.H. Coles, I.D. Campbell, D.A. Calderwood, and J. Ylänne. 2007. *Structure of three tandem filamin domains reveals auto-inhibition of ligand binding*. EMBO J. 26:3993-4004.

Lakowicz, J. R. 2006. *Principles of Fluorescence Spectroscopy*. 3rd edition. Springer Science+Business Media LLC, New York, USA. ISBN-13: 978-0387-31278-1. Chapter 13:460-472.

Lehtonen, J.V., D.J. Still, V.V. Rantanen, J. Ekholm, D. Björklund, Z. Iftikhar, M. Huhtala, S. Repo, A. Jussila, J. Jaakkola, O. Pentikäinen, T. Nyrönen, T. Salminen, M. Gyllenberg, and M.S. Johnson. 2004. *BODIL: a molecular modeling environment for structure-function analysis and drug design*. J.Comput.Aided Mol.Des. 18:401-419.

Li, M., J.C. Bermak, Z.W. Wang, and Q.Y. Zhou. 2000. Modulation of dopamine D(2) receptor signaling by actin-binding protein (ABP-280). Mol.Pharmacol. 57:446-452.

Lin, R., K. Karpa, N. Kabbani, P. Goldman-Rakic, and R. Levenson. 2001. *Dopamine D2 and D3 receptors are linked to the actin cytoskeleton via interaction with filamin A*. Proc.Natl.Acad.Sci.U.S.A. 98:5258-5263.

Loy, C.J., K.S. Sim, and E.L. Yong. 2003. *Filamin-A fragment localizes to the nucleus to regulate androgen receptor and coactivator functions*. Proc.Natl.Acad.Sci. 100:4562-7.

Murray, J.T., D.G. Campbell, M. Peggie, A. Mora, and P. Cohen. 2004. *Identification of filamin C as a new physiological substrate of PKBalpha using KESTREL*. Biochem.J. 384:489-494.

Nakamura, F., J.H. Hartwig, T.P. Stossel, and P.T. Szymanski. 2005. *Ca^{2+} and calmodulin regulate the binding of filamin A to actin filaments*. J.Biol.Chem. 280:32426-32433.

Nakamura, F., O. Heikkinen, O.T. Pentikäinen, T.M. Osborn, K.E. Kasza, D.A. Weitz, O. Kupiainen, P. Permi, I. Kilpeläinen, J. Ylänne, J.H. Hartwig, and T.P. Stossel. 2009. *Molecular basis of filamin A-FilGAP interaction and its impairment in congenital disorders associated with filamin A mutations*. PLoS One. 4:e4928.

Ohta, Y., and J.H. Hartwig. 1995. *Actin filament crosslinking by chicken gizzard filamin is regulated by phosphorylation in vitro*. Biochemistry. 34:6745-6754.

Ohta, Y., J.H. Hartwig, and T.P. Stossel. 2006. *FilGAP, a Rho- and ROCK-regulated GAP for Rac binds filamin A to control actin remodelling*. Nat.Cell Biol. 8:803-814.

Ohta, Y., T.P. Stossel, and J.H. Hartwig. 1991. *Ligand-sensitive binding of actin-binding protein to immunoglobulin G Fc receptor I (FcγRI)*. Cell. 67:275-282.

Ohta, Y., N. Suzuki, S. Nakamura, J.H. Hartwig, and T.P. Stossel. 1999. *The small GTPase RalA targets filamin to induce filopodia*. Proc.Natl.Acad.Sci.U.S.A. 96:2122-2128.

Ott, I., E.G. Fischer, Y. Miyagi, B.M. Mueller, and W. Ruf. 1998. *A role for tissue factor in cell adhesion and migration mediated by interaction with actin-binding protein 280*. J.Cell Biol. 140:1241-1253.

Ozanne, D.M., M.E. Brady, S. Cook, L. Gaughan, D.E. Neal, and C.N. Robson. 2000. *Androgen receptor nuclear translocation is facilitated by the f-actin crosslinking protein filamin*. Mol.Endocrinol. 14:1618-1626.

Pentikäinen, U., P. Jiang, H. Takala, S. Ruskamo, I. D. Campbell, and J. Ylänne. 2010. *Assembly of a filamin four domain fragment and the influence of splicing variant-1 on the structure*. Manuscript.

Pentikäinen, U., and J. Ylänne. 2009. *The regulation mechanism for the auto-inhibition of binding of human filamin A to integrin*. J.Mol.Biol. 393:644-657.

Petrecca, K., D.M. Miller, and A. Shrier. 2000. *Localization and enhanced current density of the Kv4.2 potassium channel by interaction with the actin-binding protein filamin*. J.Neurosci. 20:8736-8744.

Phillips, J.C., R. Braun, W. Wang, J. Gumbart, E. Tajkhorshid, E. Villa, C. Chipot, R.D. Skeel, L. Kale, and K. Schulten. 2005. *Scalable molecular dynamics with NAMD*. J.Comput.Chem. 26:1781-1802.

Popowicz, G.M., M. Schelicher, A.A. Noegel, and T.A. Holak. 2006. *Filamins: promiscuous organizers of the cytoskeleton*. Trends Biochem.Sci. 31:411-9.

Pudas, R., T.R. Kiema, P.J. Butler, M. Stewart, and J. Ylänne. 2005. *Structural basis for vertebrate filamin dimerization*. Structure. 13:111-119.

Ridley, A.J., M.A. Schwartz, K. Burridge, R.A. Firtel, M.H. Ginsberg, G. Borisy, J.T. Parsons, and A.R. Horwitz. 2003. *Cell migration: integrating signals from front to back*. Science. 302:1704-1709.

Robertson, S.P. 2005. *Filamin A: phenotypic diversity*. Curr.Opin.Genet.Dev. 15:301-307.

Ryckaert, J., G. Ciccotti, and H. Berendsen. 1977. *Numerical integration of the Cartesian equations of motion of a system with constraints: molecular dynamics of n-alkanes.* J.Comput.Phys. 23:327-341.

Sagui, C. and T. Darden. 1999. *P3M and PME: a comparison of the two methods. In Simulation and Theory of Electrostatic Interactions in Solution.* (Pratt, L., S. Garde, and G. Hummer, eds) pp. 104-113, American Institute of Physics, Melville, NY.

Sasaki, A., Y. Masuda, Y. Ohta, K. Ikeda, and K. Watanabe. 2001. *Filamin associates with Smads and regulates transforming growth factor-beta signaling*. J.Biol.Chem. 276:17871-17877.

Schafmeister, C., W. Ross, and V. Romanovski. 1995. *The leap module of AMBER*. University of California, San Francisco.

Schlick, T., R. Skeel, A. Brunger, L. Kale, J.J. Board, J. Hermans, and K. Schulte. 1999. *Algorithmic challenges in computational molecular biophysics*. J.Comput.Phys. 151:9-48.

Schwaiger, I., A. Kardinal, M. Schleicher, A.A. Noegel, and M. Rief. 2004. *A mechanical unfolding intermediate in an actin-crosslinking protein.* Nat.Struct.Mol.Biol. 11:81-85.

Sheen, V.L., Y. Feng, D. Graham, T. Takafuta, S.S. Shapiro, and C.A. Walsh. 2002. *Filamin A and Filamin B are co-expressed within neurons during periods of neuronal migration and can physically interact.* Hum.Mol.Genet. 11:2845-2854.

Seo, M.D., S.H. Seok, H. Im, A.R. Kwon, S.J. Lee, H.R. Kim, Y. Cho, D. Park, and B.J. Lee. 2009. *Crystal structure of the dimerization domain of human filamin A*. Proteins. 75:258-263.

Stevens, N., J. Dyer, A.A. Marti, M. Solomon, and N.J. Turro. 2007. *FRETView: a computer program to simplify the process of obtaining fluorescence resonance energy transfer parameters*. Photochem.Photobiol.Sci. 6:909-911.

Tadokoro, S., S.J. Shattil, K. Eto, V. Tai, R.C. Liddington, J.M. de Pereda, M.H. Ginsberg, and D.A. Calderwood. 2003. *Talin binding to integrin beta tails: a final common step in integrin activation*. Science. 302:103-106.

Takafuta, T., M. Saeki, T.T. Fujimoto, K. Fujimura, and S.S. Shapiro. 2003. *A new member of the LIM protein family binds to filamin B and localizes at stress fibers*. J.Biol.Chem. 278:12175-12181.

Tavano, R., R.L. Contento, S.J. Baranda, M. Soligo, L. Tuosto, S. Manes, and A. Viola. 2006. *CD28 interaction with filamin-A controls lipid raft accumulation at the T-cell immunological synapse*. Nat.Cell Biol. 8:1270-1276.

Thompson, T.G., Y.M. Chan, A.A. Hack, M. Brosius, M. Rajala, H.G. Lidov, E.M. McNally, S. Watkins, and L.M. Kunkel. 2000. *Filamin 2 (FLN2): A muscle-specific sarcoglycan interacting protein*. J.Cell Biol. 148:115-126.

Toukmaji, A., C. Sagui, J. Board, and T. Darden. 2000. *Efficient particle-mesh Ewald based approach to fixed and induced dipolar interactions.* J.Chem.Phys. 113:10913-10927.

Tu, Y., S. Wu, X. Shi, K. Chen, and C. Wu. 2003. *Migfilin and Mig-2 link focal adhesions to filamin and the actin cytoskeleton and function in cell shape modulation*. Cell. 113:37-47.

Vadlamudi, R.K., F. Li, L. Adam, D. Ngyuen, Y. Ohta, T.P. Stossel, and R. Kumar. 2002. *Filamin is essential in actin cytoskeletal assembly mediated by p21-activated kinase 1*. Nat.Cell Biol. 4:681-90.

van der Flier, A., I. Kuikman, D. Kramer, D. Geerts, M. Kreft, T. Takafuta, S.S. Shapiro, and A. Sonnenberg. 2002. *Different splice variants of filamin-B affect myogenesis, subcellular distribution, and determine binding to integrin* β *subunits*. J.Cell Biol. 156:361-376.

van der Flier, A., and A. Sonnenberg. 2001. *Structural and functional aspects of filamins*. Biochem. Biophys.Acta. 1538:99-117.

Vorgerd, M., P.F. van der Ven, V. Bruchertseifer, T. Lowe, R.A. Kley, R. Schroder, H. Lochmuller, M. Himmel, K. Koehler, D.O. Furst, and A. Huebner. 2005. *A mutation in the dimerization domain of filamin c causes a novel type of autosomal dominant myofibrillar myopathy*. Am.J.Hum.Genet. 77:297-304.

Wang, K., J.F. Ash, and S.J. Singer. 1975. *Filamin, a new high-molecular-weight protein found in smooth muscle and non-muscle cells*. Proc.Natl.Acad.Sci.U.S.A. 72:4483-4486.

Wouters, F.S., P.J. Verveer, and P.I. Bastiaens. 2001. *Imaging biochemistry inside cells*. Trends Cell Biol. 11:203-211.

Xiang, J. Z. 2002. *JACKAL: A Protein Structure Modeling Package*. Columbia University, New York.

Yang, F., L.G. Moss, and G.N. Phillips Jr. 1996. *The molecular structure of green fluorescent protein*. Nat.Biotechnol. 14:1246-1251.

Yuan, Y. and Z. Shen. 2001. *Interaction with BRCA2 suggests a role for filamin-1 (hsFLNa) in DNA damage response.* J.Biol.Chem. 276:48318-48324.

Zheng, L., H.J. Baek, G. Karsenty, and M.J. Justice. 2007. *Filamin B represses chondrocyte hypertrophy in a Runx2/Smad3-dependent manner*. J.Cell Biol. 178:121-128.

Zhou, A.X., J.H. Hartwig, and L.M. Akyurek. 2010. *Filamins in cell signaling, transcription and organ development*. Trends Cell Biol. 20:113-123.

Zhou, X., J. Boren, and L.M. Akyurek. 2007. *Filamins in cardiovascular development*. Trends Cardiovasc.Med. 17:222-229.

GEL FILTRATION PROGRAM

0 ml	sample injection
5 ml	sample load
100 ml	start fraction collection (á 2 ml)
240 ml	end fraction collection
310 ml	end program

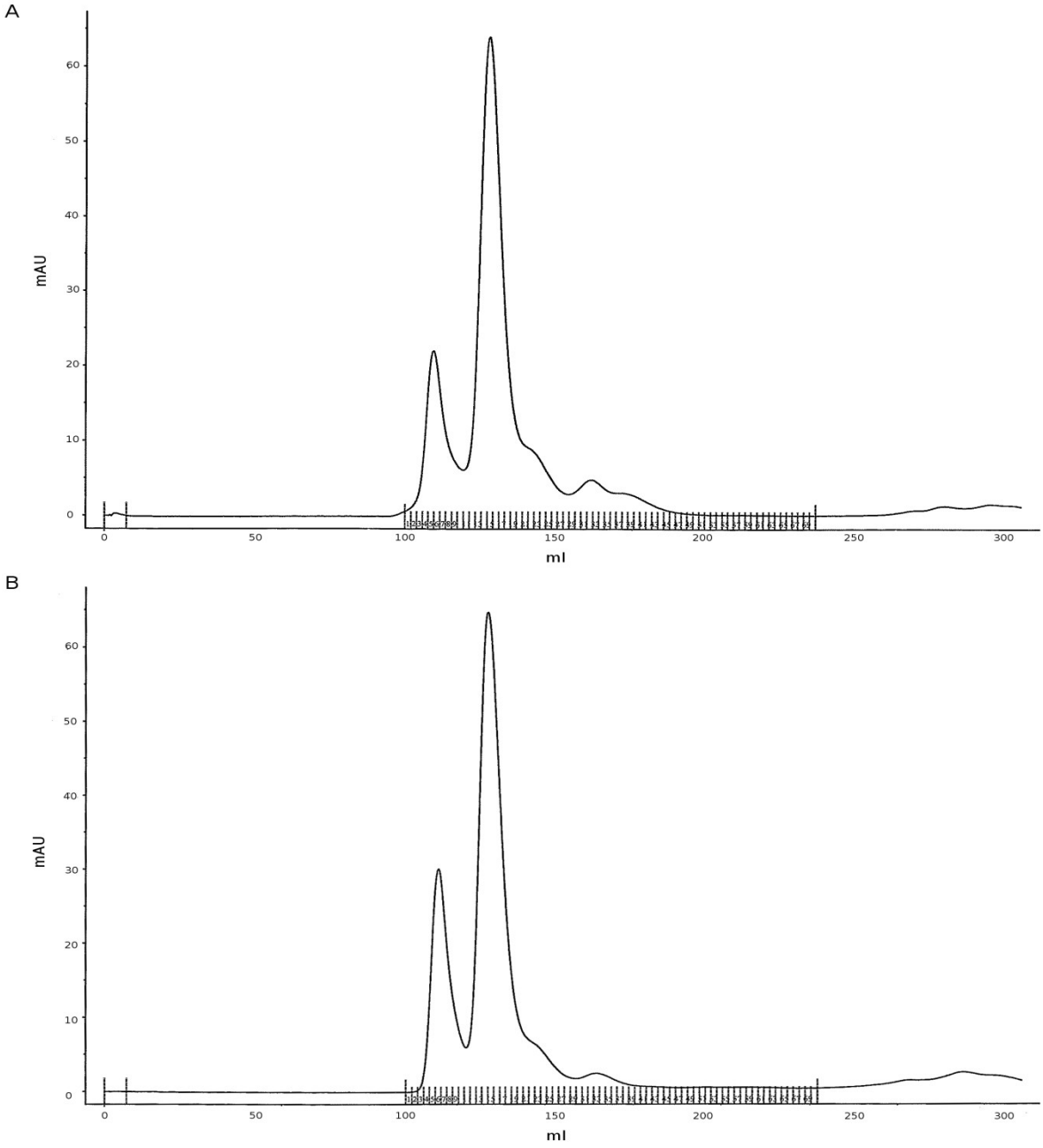

Chromatograms for the gel filtration of FLNa18-21-EGFP. (A) C2107 and (B) S2131C. The used gel filtration program is shown above. The detection wavelength was 280 nm.